Supporting Information

for

A Flexible, Redox-Active Macrocycle Enables the Electrocatalytic Reduction of Nitrate to Ammonia by a Cobalt Complex

Song Xu, Daniel C. Ashley, Hyuk-Yong Kwon, Gabrielle R. Ware, Chun-Hsing Chen, Yaroslav Losovyj, Xinfeng Gao, Elena Jakubikova, Jeremy M. Smith

25th May 2018
Note added after first publication: This supplementary information file replaces that originally published in which there were minor formatting issues in some figures and some information regarding the computer modeling was missing.

Table of Contents

Experimental Section

General Considerations

All anaerobic manipulations, including non-aqueous electrochemical measurements, were performed under a nitrogen atmosphere using standard Schlenk techniques or in an MBraun Labmaster glovebox. Deionized water was used for all aqueous experiments or measurements. All reagents were purchased from commercial venders and used as received. 1D ^{1}H NMR data were recorded on a Varian Inova 400 MHz spectrometer and 2D NMR data on Varian Inova 600 MHz NMR spectrometer at 22 ºC. UV-visible spectra were recorded with an Agilent Cary 60 UV-visible spectrometer. Mass spectra were recorded using positive electrospray ionization on a Thermo Electron Corp MAT-95XP spectrometer. Ammonia[1] and hydroxylamine[2] were analyzed according to literature protocols. Potentiometric titrations were performed at 25.0 ºC on a Mettler Toledo pH meter. The NaOH solutions for titration experiments were freshly prepared using deionized water to minimize carbonate formation.

Physical Methods

Electrochemical measurements were recorded on a CHI 600D electrochemical analyzer (CH Instruments). Cyclic voltammetry experiments were carried out in an argon purged, air-tight, single compartment cell while controlled-potential experiments (CPE) electrolysis experiments were carried out in a two compartment cell. Working electrode: glassy carbon electrode (3×3 mm^2, CH Instruments) for cyclic voltammetry, carbon rod electrode (0.5 cm in diameter, 5 cm in length) for CPE. Auxiliary electrode: platinum wire (Alfa Aesar, 99.99%). Pseudo-reference electrode: Ag wire (Alfa Asear, 99.99%) for non-aqueous solution and Ag/AgCl (CH Instruments, 1M KCl, -0.006 V vs SCE) for aqueous solution. The final redox potentials measured under non-aqueous conditions were calculated by comparing the measured potentials with $E_{1/2}$ of Fc^+/Fc in the same

solution. The reproducibility of all cyclic voltammetry experiments are verified by several repeated scans. Average peak current densities calculated from multiple scans were used for quantitative kinetic studies. X-Ray photoelectron spectra (XPS) were recorded by PHI versaprobe II XPS. Dynamic light scattering was recorded by Malvem Nano-ZS instrument.

Synthesis of Compounds

$[Co(DIM)Br_2]^+$ (DIM = 2,3-dimethyl-1,4,8,11-tetraazacyclotetradeca-1,3-diene) and $[Co(TIM)Br_2]^+$ (TIM = 2,3,9,10-tetraazacyclotetradeca-1,3-diene) were prepared according to literature procedures. NMR spectrum of $[Co(DIM)Br_2]^+$ was previously reported with lower frequency instrument, resonances were not fully assigned.[3] Crystals suitable for single crystal X-ray diffraction were directly obtained by slow diffusion of diethyl ether into its MeOH solution of $[Co(DIM)Br_2]^+$.

Characterization of $[(DIM)CoBr_2]^+$: ^1H NMR (CD_3OD, 600 MHz): δ 6.02 (2H, br, NH); 4.36 (2H, d, J = -16.3 Hz, CH_b); 3.85 (2H, t, J = -16.3 Hz, J = 12.7 Hz, CH_c); 3.24 (2H, t, J = -12.1 Hz, J = 12.0 Hz, CH_f); 2.86-2.98 (6H, m, CH_g and $CH_{i\&j}$); 2.78 (6H, s, CH_a); 2.42 (2H, d, J = -16.3 Hz, CH_e) and 2.25 (2H, q, CH_d). The resonance at δ = 6.02 ppm disappears over time due to exchange with deuterium from the NMR solvent. ESI-MS (MeOH): calcd for $[(DIM)CoBr_2]^+$: ($C_{12}H_{24}CoBr_2N_4$) m/Z: 442.97 (M^+), found: 443.0. Λ_M = 578 S•cm^{-2}•mol^{-1}.

Preparation of $[Co(DIM)(NO_3)_2]^+$: A 20 mL vial (wrapped with aluminum foil) was charged with $AgNO_3$ powder (51 mg, 0.3 mmol, 3.05 eq) and a solution of $[Co(DIM)Br_2]^+$ (50 mg, 0.096 mmol) in methanol (15 mL) at ambient temperature. The resulting solution of mixture was left at room temperature with stirring. After stirred overnight, the off-white precipitate (AgBr) was removed through filtration and a brown solution was collected. The solution was dried under reduced pressure to give a red-brown powder (28 mg, 59%). Crystals suitable for single crystal X-

ray diffraction were directly obtained by slow diffusion of diethyl ether into its MeOH solution of $[(DIM)Co(NO_3)_2]^+$. ^1H NMR (CD_3OD, 400 MHz): δ 6.84 (2H, br, NH); 4.31 (2H, d, J = -17.53 Hz, CH_b); 3.74 (2H, m, CH_c); 2.90 (2H, d, J = -17.53 Hz, $CH_{i/j}$); 2.87 (6H, s, CH_a); 2.79-2.84 (2H, m, $CH_{g/f}$); 2.76 (2H, d, J = -7.36 Hz, $CH_{i/j}$); 2.65 (2H, d, J = -7.36 Hz, $CH_{g/f}$); 2.50 (4H, m, CH_d). The resonance at δ 6.84 ppm disappears over time due to exchange with deuterium from the NMR solvent. Λ_M = 638 S□cm^2□mol^{-1}.

Electrochemical Calculations

Faradaic efficiency calculation. The amount of NH_3 generated through CPE at -1.05 V vs SCE was quantified by the indophenol method.[1] Solution for CPE experiment: 0.5 mM $[Co(DIM)Br_2]^+$ and 100 mM $NaNO_3$ in H_2O (20 mL), pH = 3.5.

Ammonia quantification shows 23.6 × 10^{-3} mmol was generated by the CPE experiment. Thus, according to equation (1), 189.2 × 10^{-3} mmol electrons were used for NH_3 generation.

$$NO_3^- + 10H^+ + 8e^- \rightarrow NH_4^+ + 3H_2O \quad (1)$$

Since 18.7 C (194.78 × 10^{-3} mmol, background subtracted) electrons were consumed in total according to the total charge accumulation diagram, the Faraday efficiency can be calculated as:

(e^- used for NH_3 generation)/ (total e^- consumed) = 189.2 × 10^{-3}/194.78 × 10^{-3} = 97.1%.

After the solution (0.5 mM $[(DIM)CoBr_2]^+$ + 100 mM $NaNO_3$, 15 mL) was electrolyzed under -1.05 V *vs* SCE for 2hr, 25.7 μmol NH_3 was found by indophenol test. Since total 7.5 μmol $[(DIM)CoBr_2]^+$ was used for electrocatalysis, turnover number (TON) = 25.7/7.5 = 3.4 for the 2 h electrolysis.

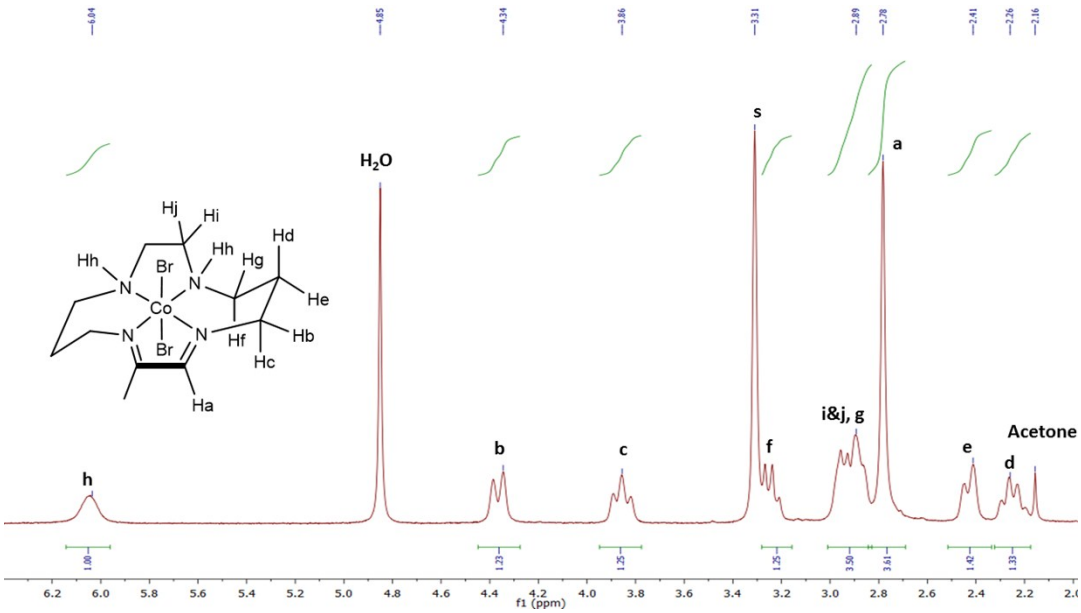

Figure S1. ^{1}H NMR spectrum of $[Co(DIM)Br_2]^+$ (solvent: CD_3OD) with peak assignments based on COSY, HSQC and NOESY spectra (Figure S2 - Figure S4), s = protio impurities in CD_3OD.

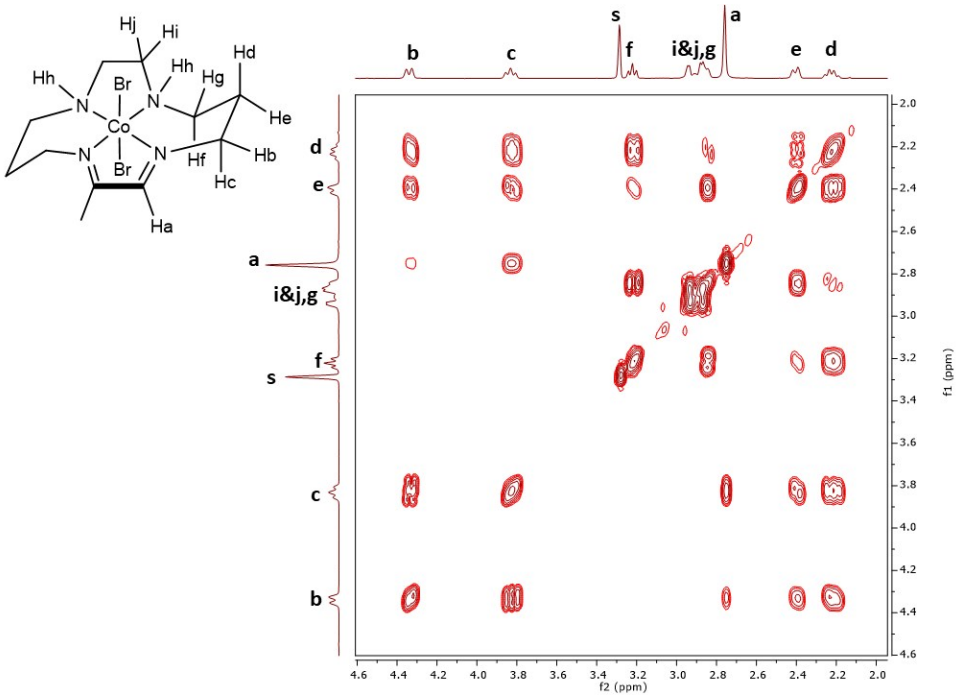

Figure S2. COSY45 NMR spectrum of $[Co(DIM)Br_2]^+$ (solvent: CD_3OD), s = protio impurities in CD_3OD.

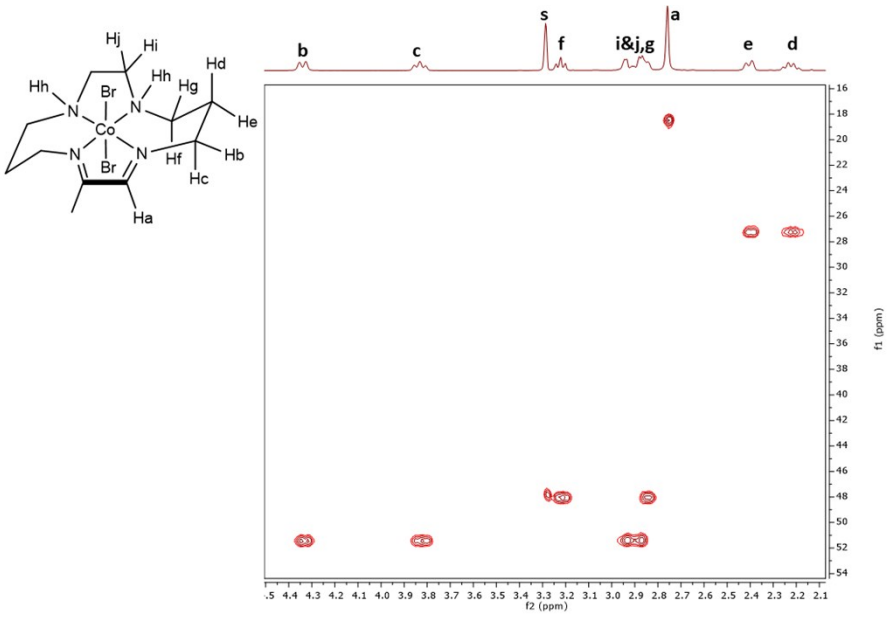

Figure S3. HSQC NMR spectrum of $[Co(DIM)Br_2]^+$ (solvent: CD_3OD), s = protio impurities in CD_3OD.

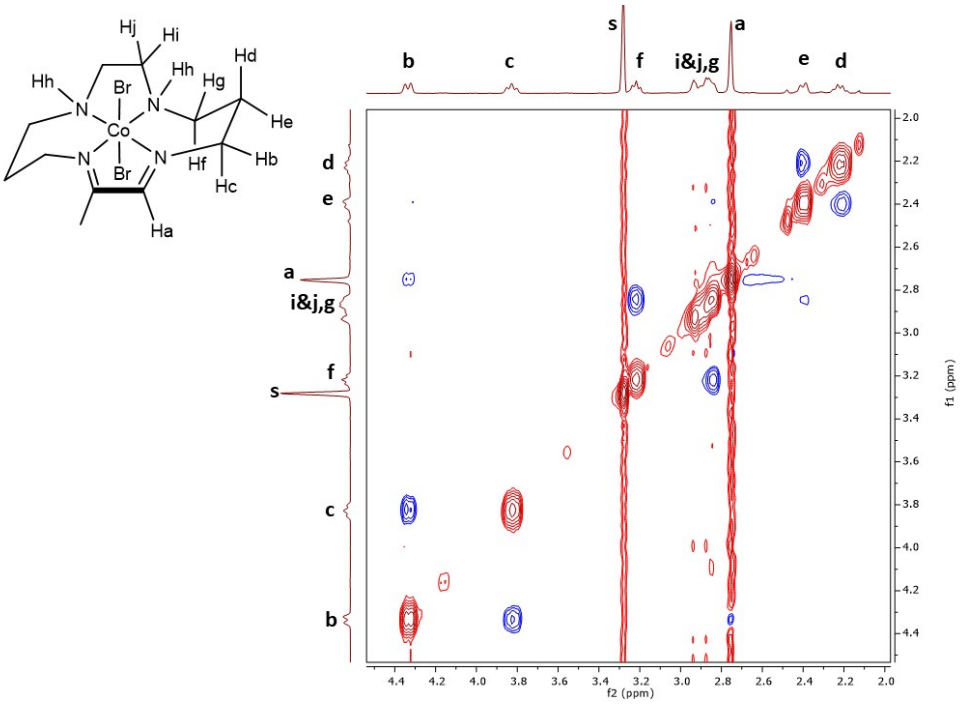

Figure S4. NOESY NMR spectrum of $[Co(DIM)Br_2]^+$ (solvent: CD_3OD), s = protio impurities in CD_3OD.

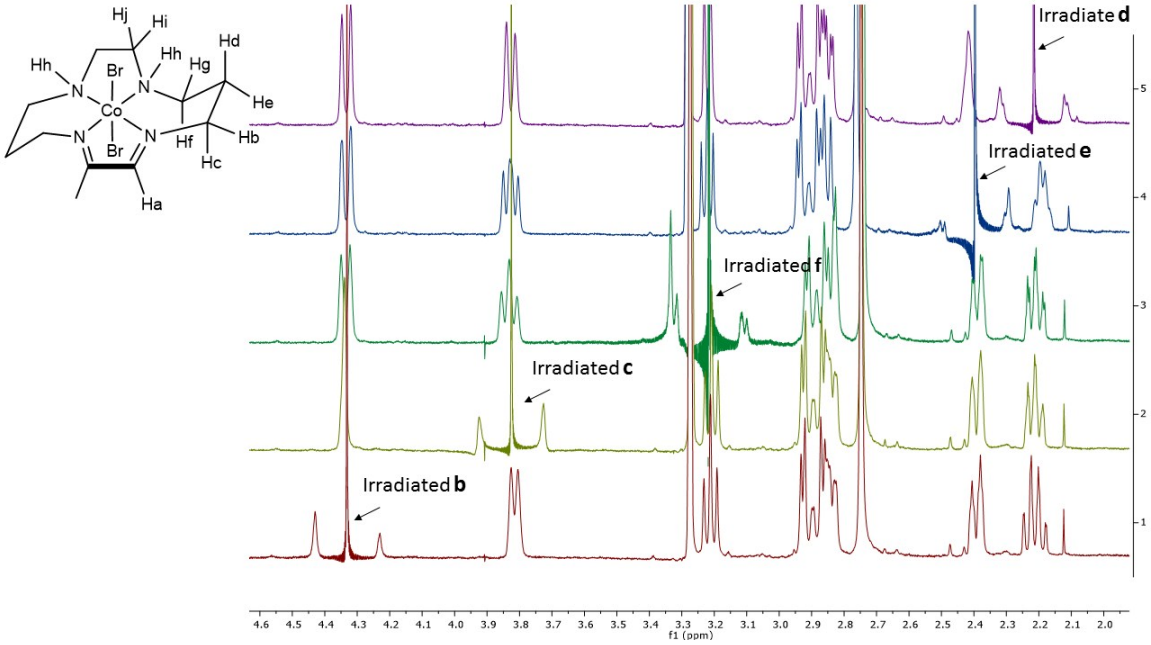

Figure S5. Homodecoupling 1H NMR spectrum of $[Co(DIM)Br_2]^+$.

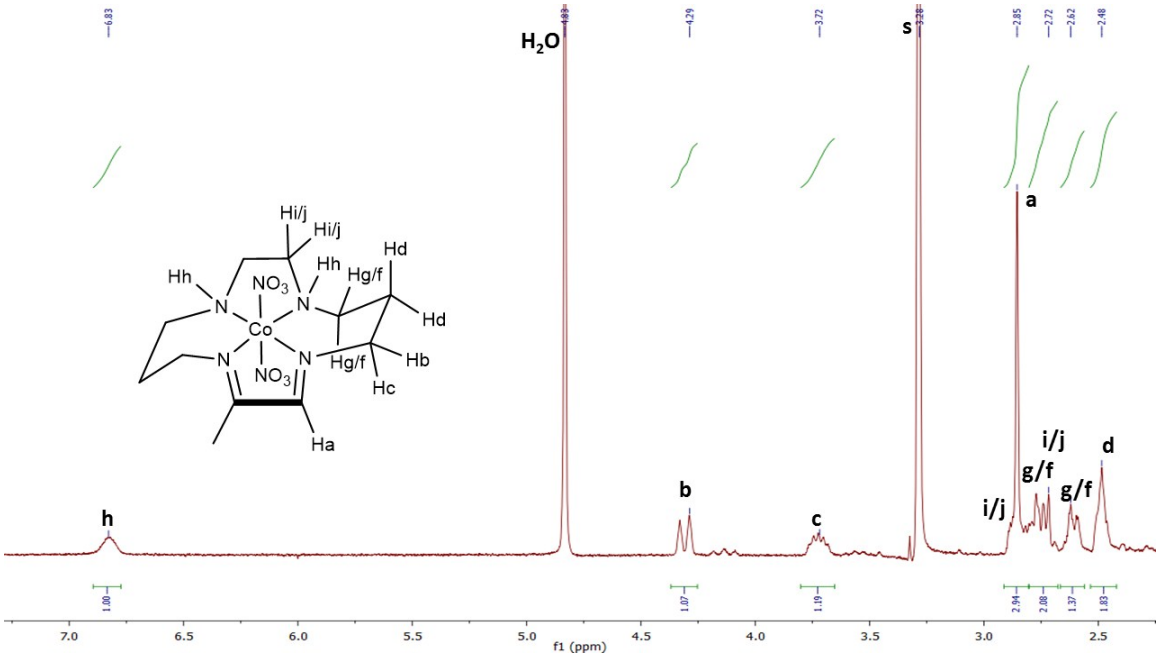

Figure S6. ^1H NMR spectrum of $[Co(DIM)(NO_3)_2]^+$ (solvent: CD_3OD),), s = protio impurities in CD_3OD.

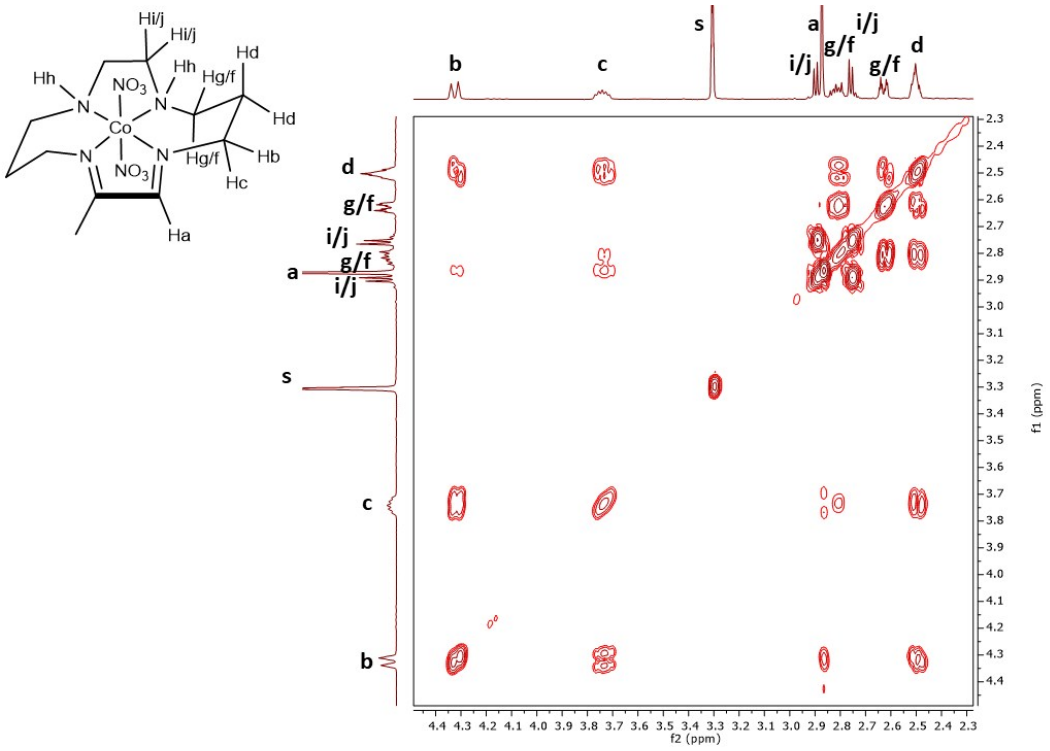

Figure S7. COSY45 NMR spectrum of $[Co(DIM)(NO_3)_2]^+$ (solvent: CD_3OD), s = protio impurities in CD_3OD.

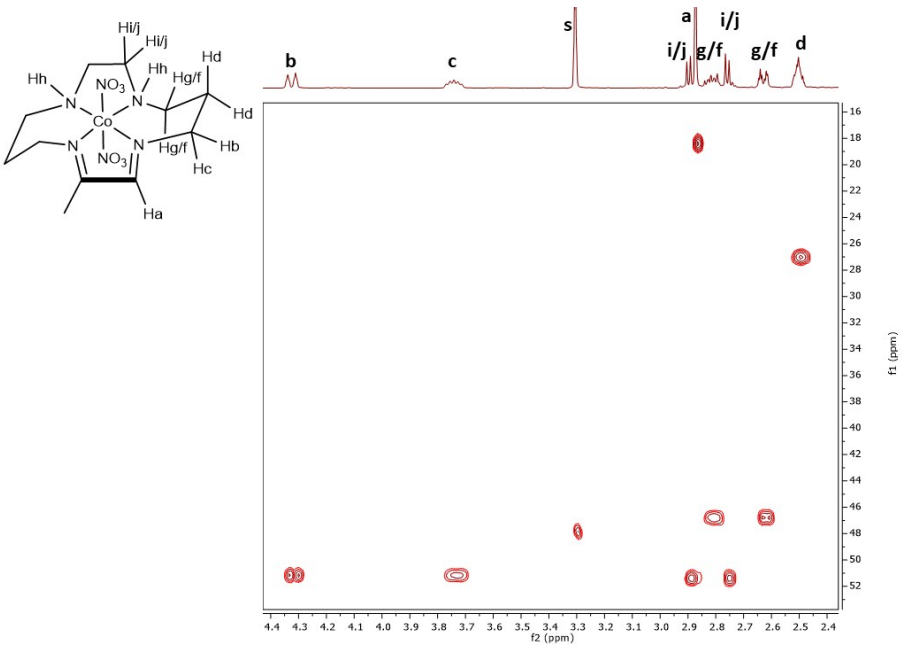

Figure S8. HSQC NMR spectrum of $[Co(DIM)(NO_3)_2]^+$ (solvent: CD_3OD), s = protio impurities in CD_3OD.

Spectra of Aqueous Speciation

UV-vis Spectroscopy. The UV-vis spectra of $[Co(DIM)Br_2]^+$ in MeOH and H_2O (Figure S9a) suggest the bromide ligands are hydrolyzed in aqueous solution. Hydrolysis is reversible, as revealed by the spectral changes when an aqueous solution of $[Co(DIM)Br_2]^+$ is titrated with Br^- (Figure S9b).

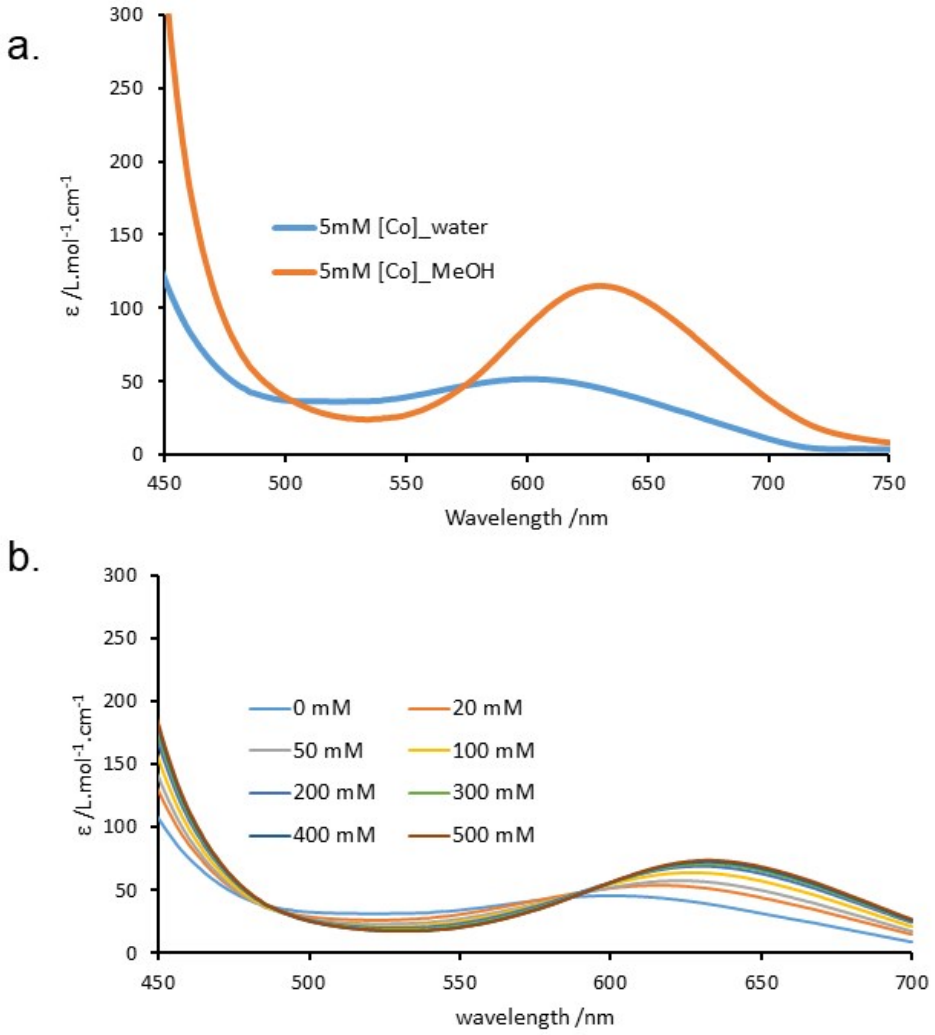

Figure S9. (a): UV-vis spectra of $[Co(DIM)Br_2]^+$ in MeOH (orange) and H_2O (blue). (b): UV-vis spectra of 2.5 mM $[Co(DIM)Br_2]^+$ in H_2O with different concentration of KBr.

^{1}H NMR spectroscopy in D_2O. In contrast to $[Co(DIM)(NO_3)_2]^+$, which shows a single resonance at δ 2.95 ppm for the DIM methyl groups, two such resonances (δ 2.88 ppm and δ 2.81 ppm) are observed in the ^{1}H NMR spectrum of $[Co(DIM)Br_2]^+$ in D_2O (Figure S10). It is notable that the chemical shift for the methyl groups in $[Co(DIM)(NO_3)_2]^+$ is different from those observed for $[Co(DIM)Br_2]^+$. This suggests that at least two different species are present in aqueous solutions of $[Co(DIM)Br_2]^+$.

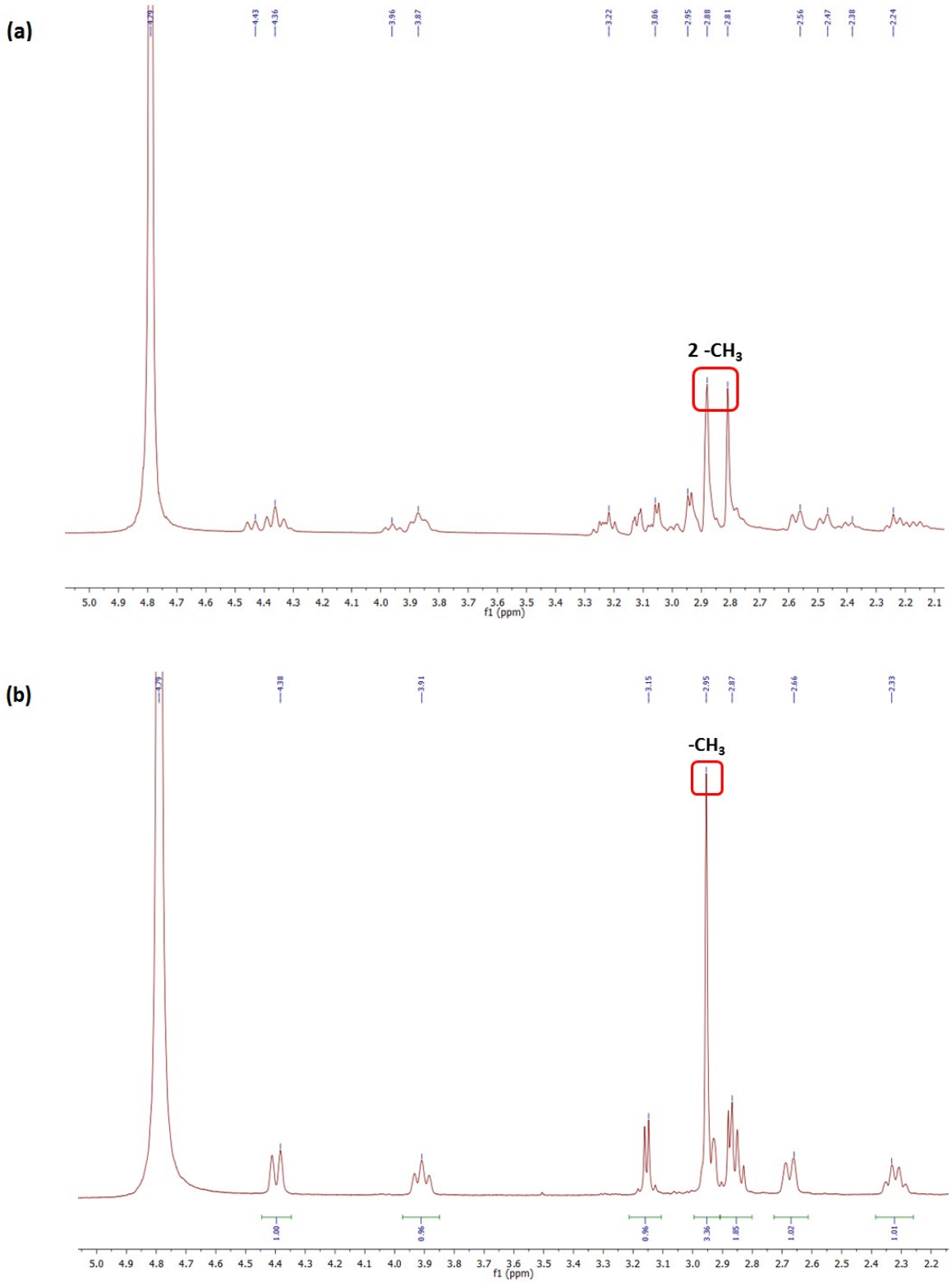

Figure S10. ^{1}H NMR spectra of $[Co(DIM)Br_2]^+$ (top) and $[Co(DIM)(NO_3)_2]^+$ (bottom) in D_2O.

pH Titration. The initial pH of 2.5 mM solutions of both $[(DIM)CoBr_2]^+$ and $[(DIM)Co(NO_3)_2]^+$ are acidic (pH = 3.2 for $[(DIM)CoBr_2]^+$ and 2.78 for $[(DIM)Co(NO_3)_2]^+$, consistent with proton loss from ligands. Two pK_a's are observed for both $[(DIM)CoBr_2]^+$ (pK_a1 = 5.2, pK_a2 = 9.0. Figure S11a) and $[(DIM)Co(NO_3)_2]^+$ (pK_a1 = 5.0, pK_a2 = 9.0. Figure S11b).

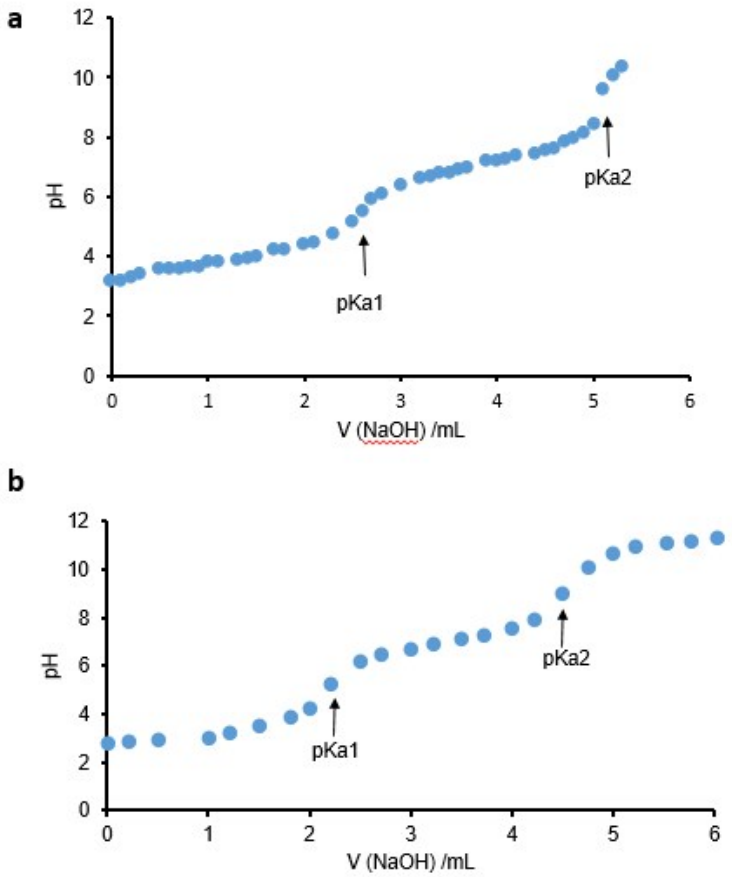

Figure S11. Titration of 50 mL, 2.5 mM $[(DIM)CoBr_2]^+$ **(a)** and $[(DIM)Co(NO_3)_2]^+$ **(b)** with 50 mM NaOH solution.

Electrocatalytic Activity of $[Co(DIM)Br_2]^+$ and $[Co(DIM)(NO_3)_2]^+$.

The cyclic voltammograms of $[Co(DIM)(NO_3)_2]^+$ and $[Co(DIM)Br_2]^+$ in the presence of nitrate are similar (Figure S12), indicating that both complexes provide access to the same active species for NO_3^- reduction.

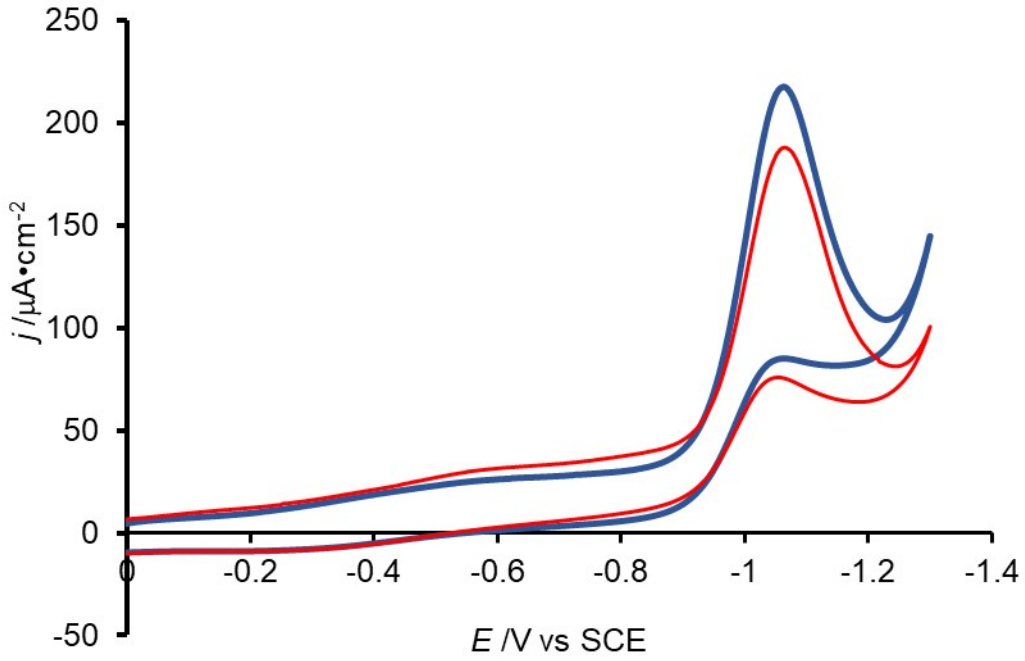

Figure S12. Cyclic voltammograms of $[Co(DIM)Br_2]^+$ (red) and $[Co(DIM)(NO_3)_2]^+$ (blue) with 10 mM $NaNO_3$. GC electrode, scan rate = 5 mV/s, pH = 4.3.

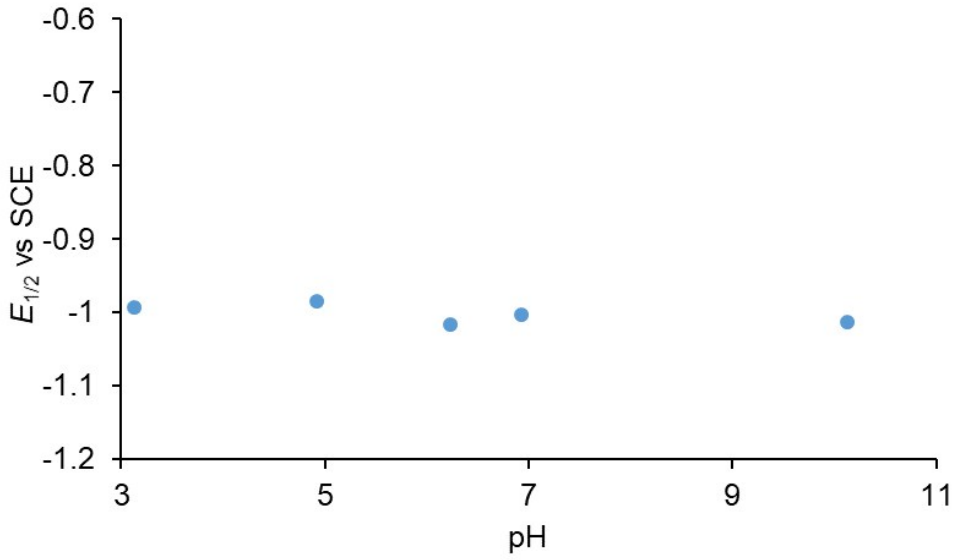

Figure S13. $E_{1/2}$ of 0.5 mM $[Co(DIM)(NO_3)_2]^+$ with 50 mM Na_2SO_4 in H_2O solution with different pH. GC electrode, scan rate = 2000 mV/s.

Foot of the Wave Analysis (FOWA)

Since we were unable to attain purely kinetic conditions, we used the FOWA to determine the rate law for the first chemical step of electrocatalysis.[4-5] The FOWA plots the catalytic current density *vs.* normalized potential, exp(-F/RT(E-E_{redox})), see Fig. S14, where E_{redox} corresponds to the Co(DIM)/Co(DIM)$^-$ couple. Since the slope of each FOWA curve of Figure S14 is equal to $2FAC_P^0\sqrt{D}\sqrt{kC_A^0}$,[4] linear relationships are expected to be observed by plotting slope of each curve vs. C_P^0 (catalyst concentration) and C_A^0 (substrate concentration) (Figure 8, insets). Since we do not know the Co(DIM)/Co(DIM)$^-$ potential, we have approximated it as E_{redox} -1.05 V vs SCE, which is likely to be the two electron couple, based on the computational studies. The real potential for the Co(DIM)/Co(DIM)$^-$ wave will be less negative than this value by an unknown amount. Test calculations show that the value chosen for E_{redox} does not affect the conclusions regarding the dependence of the catalytic rate on the concentration of catalyst, nitrate or protons in the FOWA. However, the value of E_{redox} has a significant impact on the values obtained for the rate constant. For this reason, we are not confident in reporting rate constants from the electrochemical experiments and we cannot reliably determine the TOF.

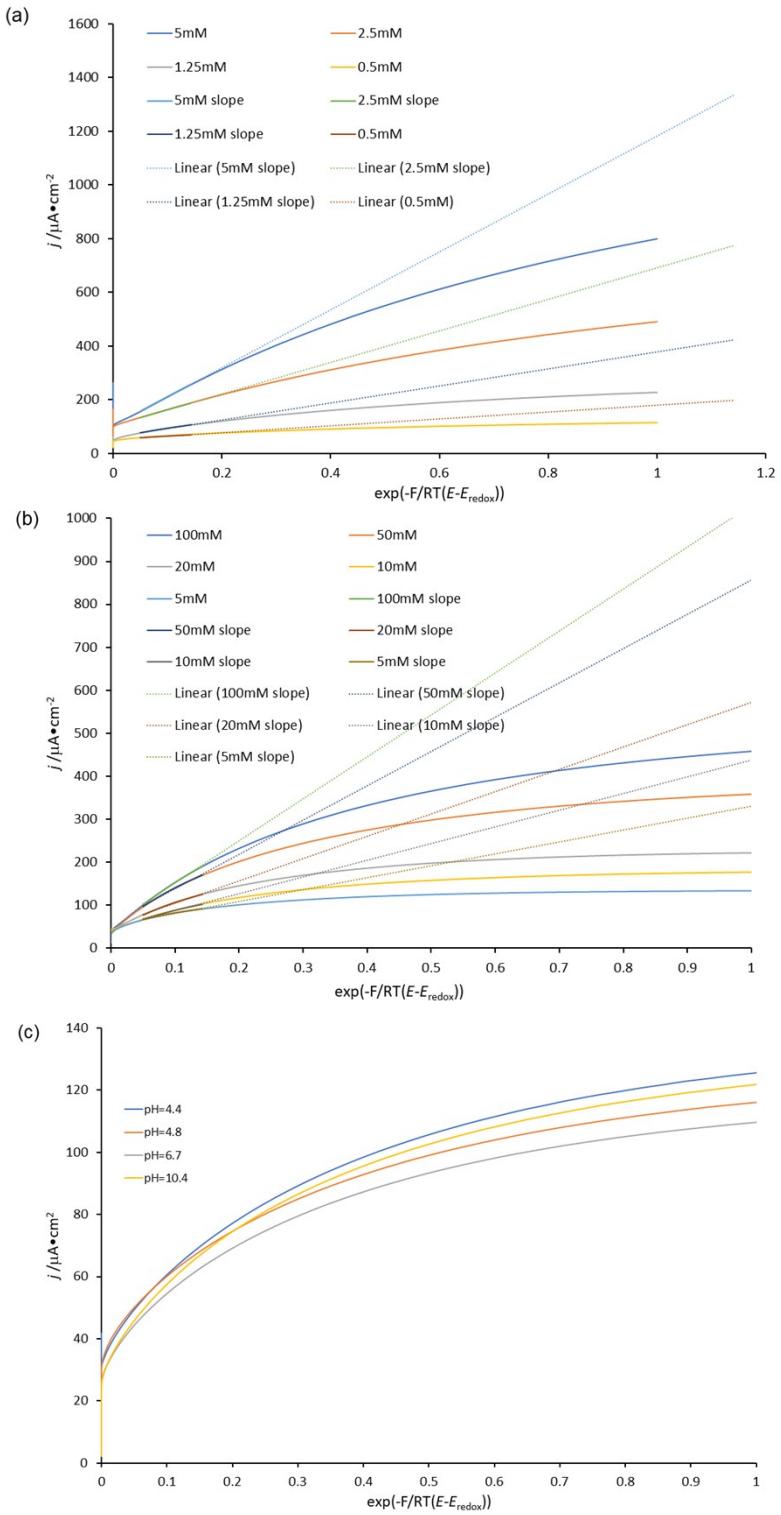

Figure S14. Foot of wave analysis (FOWA) of catalytic NO_3^- reduction by $[(DIM)CoBr_2]^+$ under different concentrations of (a) $[(DIM)CoBr_2]^+$ (catalyst), (b) $[NO_3^-]$ (substrate) and (c) $[H^+]$. The slope for the FOWA = $2FAC_p\sqrt{D}\sqrt{k_1C_A}$, which was used in Figure 8, inset.

Substrate Selectivity

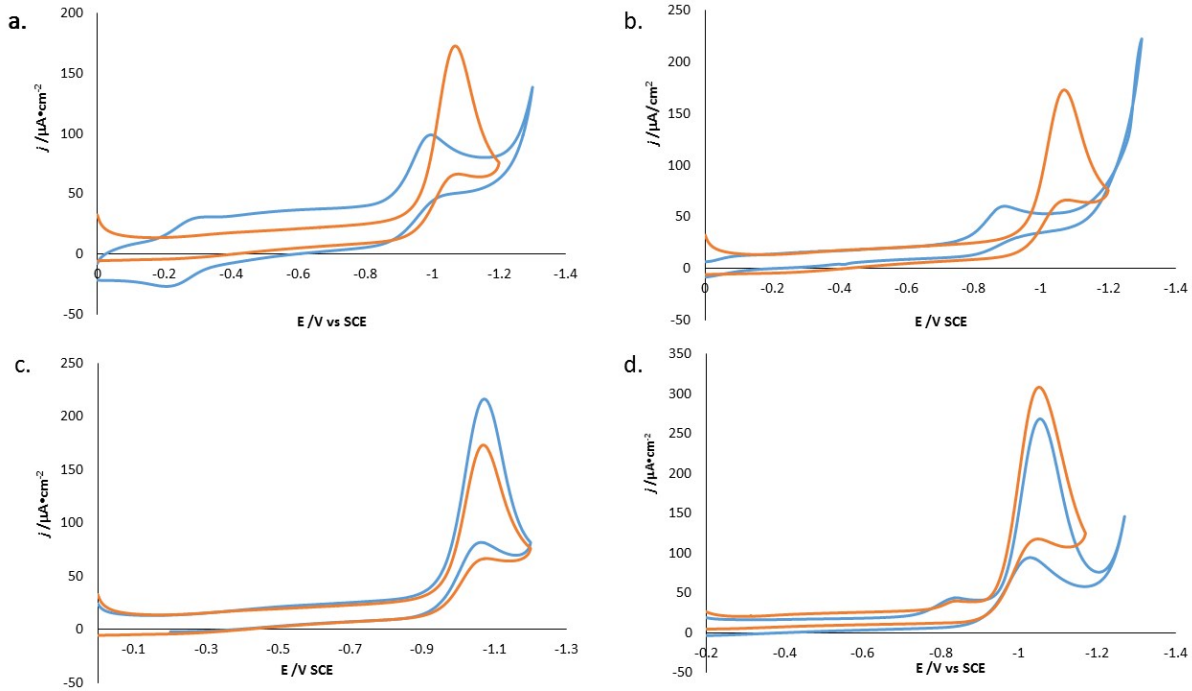

Figure S15. (a) CV of 0.5 mM $[Co(DIM)Br_2]^+$ with 10 mM $NaNO_3$ in the presence of 10 mM $NaHCO_3$ (blue) and 50 mM KBr (orange), pH = 6.4; **(b)** CV of 0.5 mM $[Co(DIM)Br_2]^+$ with 10 mM $NaNO_3$ in the presence of 10 mM NaH_2PO_4 (blue) and 50 mM KBr (orange), pH = 6.7; **(c)** CV of 0.5 mM $[Co(DIM)Br_2]^+$ with 10 mM $NaNO_3$ in the presence of 50 mM KOTf (blue) and 50 mM KBr (orange), pH = 4.6; **(d)** CV of 0.5 mM $[(DIM)CoBr_2]^+$ with 100 mM $NaNO_3$ in the presence of 100 mM Na_2SO_4 (blue) and 100 mM KBr (orange), pH = 4.1. Working electrode: glassy carbon.

Tests for Catalyst Homogeneity

X-ray Photoelectron Spectroscopy (XPS). It has been reported that during the catalysis of nitrate reduction catalyzed by $[Co(cyclam)Cl_2]^+$, the catalyst is absorbed on the surface of electrode, with the intactness of the catalyst confirmed through XPS.[6]

XPS was similarly used to investigate the homogeneity of the $[Co(DIM)Br_2]^+$ catalyst. Following several CV scans of an aqueous $[Co(DIM)Br_2]^+$ solution with NO_3^- substrates, the GC electrode is gently rinsed with deionized water, and the surface is analyzed by XPS. These measurements revealed small amounts of Co and N (Figure S16), with overall ratio C: 98.4%, N: 1.5%, Co: 0.2%. It is notable that all the N is consistent with N^{-III} (N of DIM ligand) and not N^{V} (N of NO_3^-), suggesting that the rinse removed soluble compounds such as NO_3^-.[7] No Br was found on the electrode surface, consistent with the aqueous speciation studies (see above). Overall, the XPS experiments suggest that small amount of catalyst is adsorbed on the surface of electrode while most of the catalyst, electrolyte, substrate and reduction product are soluble and washed off by the gentle rinse.

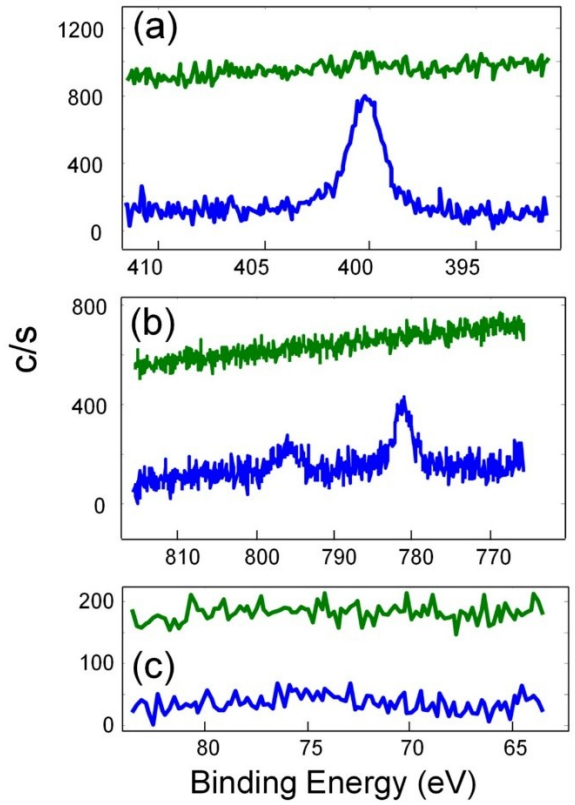

Figure S16. High resolution X-ray photoelectron spectra of N 1s (a), Co 2p (b) and Br 3d (c) regions of glassy carbon electrode after six scans of catalytic NO_3^- reduction from 0 to -1.3 V vs SCE. Solution: 0.5 mM $[Co(DIM)Br_2]^+$, 10 mM $NaNO_3$ and 50 mM KBr (blue curves). Green curves after the electrode was polished with Al_2O_3 powder and sonicated.

Rinse Test. A rinse test was also undertaken to further detect possible active catalyst deposition at the electrode surface. After several scans of a solution containing 0.5 mM $[Co(DIM)Br_2]^+$, 10 mM $NaNO_3$ and 50 mM KBr, the GC electrode is gently washed and used to scan the CV in a solution with 10 mM $NaNO_3$ and 50 mM KBr only. No catalytic current is observed after the rinse, which indicates that no sufficient active catalyst deposited on the electrode (Figure S16).

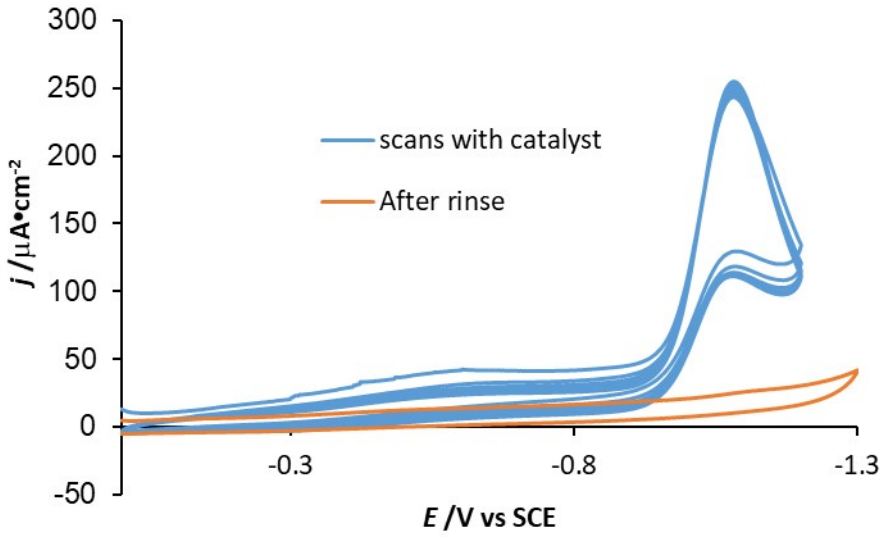

Figure S17. Cyclic voltammograms of 0.5 mM $[Co(DIM)Br_2]^+$ and 10 mM $NaNO_3$ (6 scans, blue) and 10 mM $NaNO_3$ with rinsed electrode right after CV experiments with catalyst (orange), electrolyte: 50 mM KBr. Glassy carbon electrode, pH = 4.3, scan rate = 5 mV/s.

Dynamic Light Scattering (DLS) and UV-vis. DLS and UV-vis experiments were used to test for nanoparticle formation following electrolysis of 0.5 mM $[Co(DIM)Br_2]^+$ solution with 100 mM $NaNO_3$ (10 min electrolysis, -1.05 V vs SCE) . DLS measurements with 0.002% standard latex as reference (Figure S18) did not show evidence for nanoparticle formation following electrolysis. Additionally, no new bands are observed in the UV-vis spectrum (Figure S19) following electrolysis, also suggesting that no nanoparticles are formed.

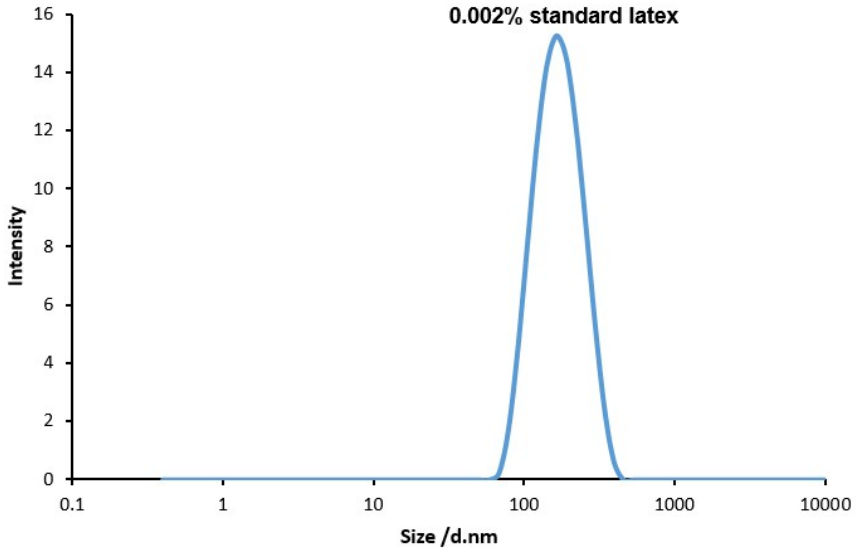

Figure S18. Dynamic light scattering studies of 0.5 mM $[Co(DIM)Br_2]^+$ + 100 mM $NaNO_3$ after electrolyzed for 10 min at -1.1 V vs SCE (Initial pH = 3.5, 0.002% standard latex is added for reference).

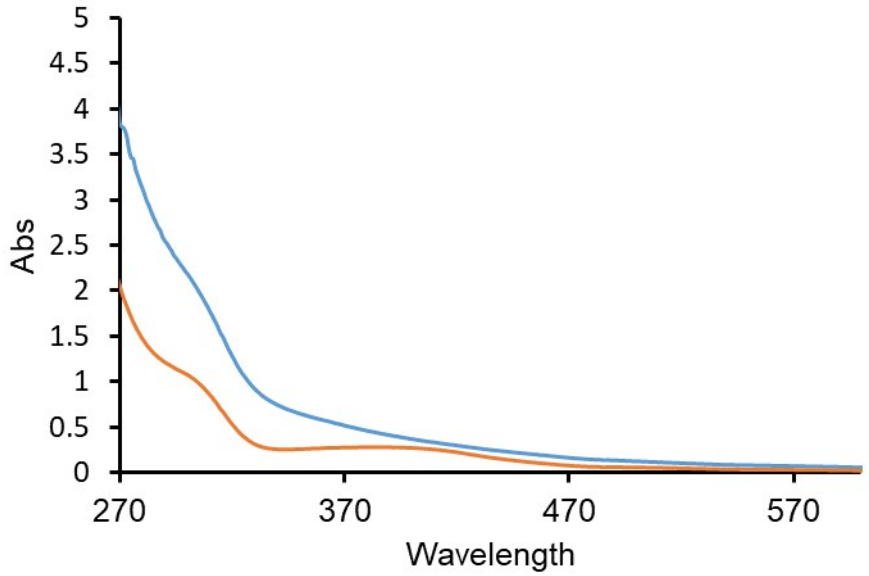

Figure S19. UV-vis spectra of 0.5 mM $[Co(DIM)Br_2]^+$ + 100 mM $NaNO_3$ before electrolysis (orange) and after electrolyzed for 10 min (blue), initial pH = 3.5.

Macrocycle Properties

Although the overpotential is large, $[Co(DIM)Br_2]^+$ has attractive properties as an electrocatalyst for nitrate reduction. Specifically, electrocatalysis is observed under milder conditions than for $[Co(cyclam)Cl_2]^+$ and operates with a carbon electrode, without the need for a heavy metal electrode. Additionally, $[Co(DIM)Br_2]^+$ has better product selectivity, producing only ammonia, whereas $[Co(cyclam)Cl_2]^+$ produces both ammonia and hydroxylamine.[8-10] Since the potential for electrocatalysis is the same as for ligand reduction, this suggests that the redox-active diimine moiety of DIM ligand is important for the improved catalytic activity.

In addition to its redox active nature, the DIM ligand has the potential to engage in hydrogen bonding through the amine donors. To test this hypothesis, the catalytic activity of a related macrocyclic complex, $[Co(TIM)Br_2]^+$ (TIM = 2,3,9,10-tetramethyl-1,4,8,11-tetraazacyclotetradeca-1,3,8,10-tetraene) toward NO_3^- reduction was investigated. In the absence of substrate, the CV of this complex shows three waves for reduction, with the first two occurring at similar potential to those of $[Co(TIM)Br_2]^+$, suggesting that these two macrocycles have similar donor strengths. However, the CV of $[Co(TIM)Br_2]^+$ in the presence of nitrate does not show a catalytic current (Figure S20). This is consistent with the N-H groups of the DIM ligand being important for catalysis, although other factors cannot be easily ruled out.

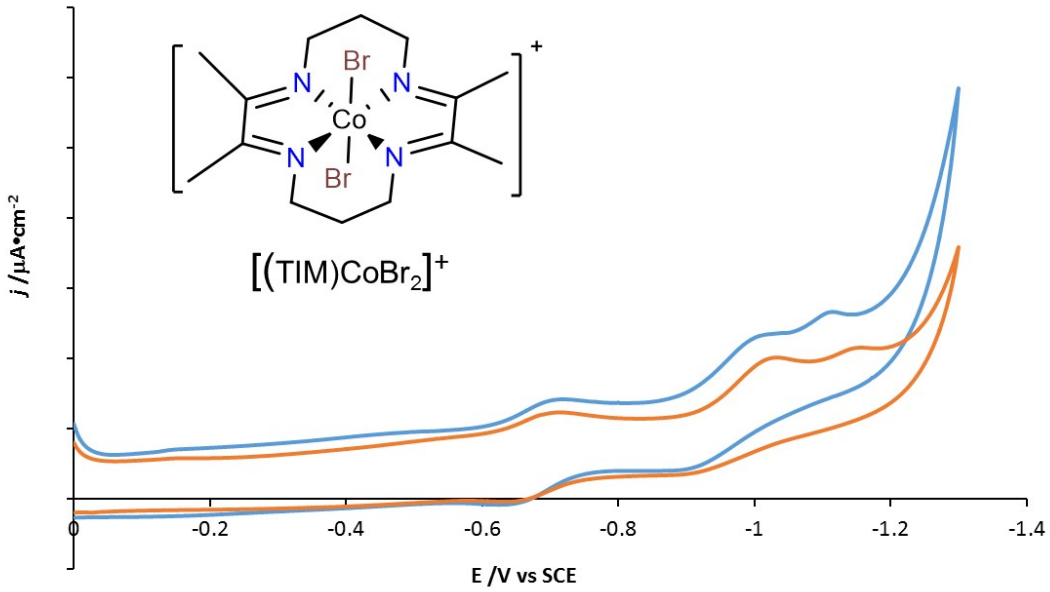

Figure S20. Cyclic voltammograms of 0.5 mM $[Co(TIM)Br_2]^+$ (orange) and 0.5 mM $[Co(TIM)Br_2]^+$ + 10 mM $NaNO_3$ (blue), GC electrode, 50 mM KBr, scan rate = 5 mV/s, pH = 4.3. Structure of $[Co(TIM)Br_2]^+$ complex (inset).

Reference pK_a and Conductivity Data

Table S1. Selected pK_a values for Co(III) complexes.[a]

Complex	pK_{a1}	pK_{a2}	Reference
$[(DIM)CoBr_2]^+$	~5	~9	this work
$[(DIM)Co(NO_3)_2]^+$	~5	~9	this work
$[Co(OH_2)]^{3+}$	2.92(4)	-	11
$[Co(tn)_2(OH_2)_2]^{3+}$	4.98	-	12
cis-β$[Co(trien)(H_2O)_2]^{3+}$	5.3(5)	7.8 ± 0.1	13
cis-$[Co(NH_3)_4(OH_2)_2]^{3+}$	5.7	7.94	14
cis-$[Co(nta)(H_2O)_2]$	6.71	-	15

[a] Ligand abbreviations: tn = 1,3-diaminopropane, nta = nitrilotriacetate, trien = triethylenetetramine

Table S2. Molar conductivity of complexes in water [a]

Complex	Molar conductivity in water ($S \cdot cm^2 \cdot mol^{-1}$)
$[(DIM)CoBr_2]^+$	638
$[(DIM)Co(NO_3)_2]^+$	578
1:1	118-131
2:1	235-273
3:1	408-435
4:1	~560

[a] Literature values taken from references [16-17]

Computational Methods

General Methodology

All structures were optimized with the B3LYP[18-21] functional including Grimme's D2 dispersion correction[22] (B3LYP+D2) unless noted otherwise. These optimizations were performed using the implicit SMD[23] model (with the exception of bromide ion where the default PCM model was used, see below) to account for solvent effects using either water or acetonitrile depending on what experimental results were being compared to. Frequencies were calculated for all optimized structures using the harmonic oscillator approximation to verify that the structures were true minima with no imaginary frequencies. The results of these frequency calculations were also used to calculate zero-point energy and entropic corrections to the free energy at 298.15 K and 1.0 atm using standard statistical mechanical conventions. Additionally, wavefunction stability tests were performed on all complexes to verify the nature of the electronic state, and only complexes with stable wavefunctions were reported.

A smaller basis set (BS-I) was used for the geometry optimizations and the frequency calculations. The electronic energies were then determined from single point energy calculations performed on these geometries with a larger basis set (BS-II) that also incorporated diffuse functions. Both BS-I and BS-II employed an SDD pseudopotential (ECP10MDF) and accompanying basis set for Co.[24-25] Br was also modeled with an SDD pseudopotential (ECP10MDF) and associated cc-pVTZ-PP basis set for BS-I, while the larger aug-cc-pVTZ-PP basis set was used for BS-II.[26] All other atoms used 6-31G* for BS-I[27-28] and 6-311+G** for BS-II.[29-30] An ultrafine grid was used for all calculations. The final solvated free energy (G_{sol}) was then adjusted[31] to have the standard state concentration of 1 M or 55.5 M for water, a correction

of -1.9 and -4.3 kcal/mol, respectively. All DFT calculations were performed with the Gaussian 09 software package Revision D.01.[32]

Calculated reduction potentials (E^0) were determined relative to the normal hydrogen electrode (NHE) through equation S1:

$$E^0(eV) = -\frac{\Delta G_{sol}}{nF} - 4.28 \text{ (Eq. S1)}$$

Here, ΔG_{sol} is the change in solvated free energy upon reduction, n is the number of electrons transferred, in our case this is always one, and F is Faraday's constant. The calculated potentials are referenced to NHE by subtracting the absolute reduction potential of NHE, 4.28 V.[33] This value of NHE is determined by the aqueous solvation free energy of the proton, 265.9 kcal/mol, and this solvation energy was also used when calculating pK_as. Note that much work has been done on determining the absolute value of NHE, and not all estimates agree,[33-39] and hence our calculated values may be subject to a modest systematic error. This will have no significant effect on our major conclusions. Furthermore, we were able to successfully benchmark this methodology against experimentally known Co(III) reduction potentials as shown in the next section. The calculated values vs. NHE are reported relative to SCE (0.2412 vs. NHE)[40] or Fc/Fc^+ (0.41 vs. SCE)[41] when necessary. As mentioned above, the PCM model was used for calculating the solvated electronic energy of the bromide anion. It was found that using the SMD value for bromide resulted in worse agreement with matching the experimental data in this paper (speciation/pK_as). Furthermore, using the PCM, the solvation energy of bromide (solvated energy - gas phase energy) was calculated to be -64.51 kcal/mol. With SMD this was calculated as -53.08 kcal/mol. Given that an accurate estimate of this value is -68.3 kcal/mol,[33] it is clear that the PCM value was more accurate and should be used preferentially.

Calculated Structures vs. Experimental Crystal Structures

Table S3. Selected bond lengths and angles for calculated and experimental $[Co(DIM)Br_2]^+$ structure. Refer to Figure 1 for the atom labels.

	Calculated	Experimental
Co-Br1	2.4605 Å	2.4009(4) Å
Co-Br2	2.4598 Å	2.4040(4) Å
Co-N1	1.9430 Å	1.930(2) Å
Co-N2	1.9474 Å	1.924(2) Å
Co-N3	1.9941 Å	1.970(2) Å
Co-N4	1.9941 Å	1.975(2) Å
Br1-Co-Br2	177.190 °	177.39(2) °

Table S4. Selected bond lengths and angles for calculated and experimental $[Co(DIM)(NO_3)_2]^+$ structure. Refer to Figure 1 for the labels of atoms.

	Calculated	Experimental
Co-O1	1.9249 Å	1.919(3) Å
Co-O4	1.9287 Å	1.929(3) Å
Co-N1	1.9604 Å	1.929(2) Å
Co-N2	1.9394 Å	1.939(4) Å
Co-N3	1.9811 Å	1.964(2) Å
Co-N4	1.9839 Å	1.958(4) Å
O1-Co-O2	169.393°	169.54(1)°

Details on electronic structures of proposed intermediates

As was mentioned in the manuscript, of all the species we considered only three had calculated reduction potentials that were close to -1.0 V (see Figure 7): $[Co(DIM)(OH)Br]^{+}$ (-1.24 V), $[Co(DIM)(OH_2)OH]^{2+}$ (-0.97 V) and $[Co(DIM)(OH)_2]^{+}$ (-0.9 V). These intermediates showed both unusual and varied electronic structures, and highlighted some of the computational difficulties related to ligand dissociation in this system. For $[Co(DIM)(OH)Br]^{+/0}$, the reported value was calculated for a species in which the DIM ligand is reduced instead of the metal (i.e. it is formally Co(III)DIM(-I)). Co is preferably reduced before the DIM ligand for virtually all complexes considered, and usually the Co(III)DIM(-I) state could not be located. The alternative metal-reduced electronic state of $[Co(DIM)(OH)Br]^{0}$ was located as well, but resulted in a complex with a very long Co-Br bond (~3.2 Å), suggesting a possible ligand dissociation. While we do not consider this structure reliable, it is worth noting that it is significantly lower in energy than the structure displaying the ligand-based reduction, resulting in a calculated reduction potential of ~ -0.7 V, placing the experimental peak potential (-1.0 V) midway through these two values. While it is difficult to definitely assign the nature of $[Co(DIM)(OH)Br]^{0}$, the range of calculated reduction potentials strongly suggests that this species is relevant electrochemically. Ligand-based reduction was also found for $[Co(DIM)(OH_2)OH]^{2+}$, as metal reduction resulted in ligand loss, while the more typical metal-based reduction was determined to occur for $[Co(DIM)(OH)_2]^{+}$.

Methodology Verification

The computational methodology's ability to predict reduction potentials was tested for several Co(III) complexes that have experimentally known reversible III/II couples so as to gauge the accuracy of the calculations. The chosen complexes (see Figure S20) are all octahedral,

undergo metal-centered reduction in aqueous solution, and contain neutral nitrogenous ligands. As not all of the complexes considered in this study possess these features, we also included $[Co(DIM)Br_2]^+$, although its reduction potential had to be calculated in acetonitrile where it was measured reversibly. Table S5 lists the calculated E^0 values compares them with experiment. For each complex, the potential was calculated going from the low-spin singlet Co(III) to the high-spin quartet Co(II), as the calculations found that the quartet was slightly lower in energy than the doublet. The one exception to this was $Co(DIM)Br_2$ which was found to be a ground-state doublet. No potential spin-state equilibrium effects were accounted for so as to avoid any issues with the uncertainty of the calculated spin-state energetics. These effects are not expected to be large in this case, as previous computational work by Baik and coworkers found that for $[Co(tacn)_2]^{3+}$ spin-state equilibria had only a minor effect on the calculated reduction potential of ~0.05 V.[42]

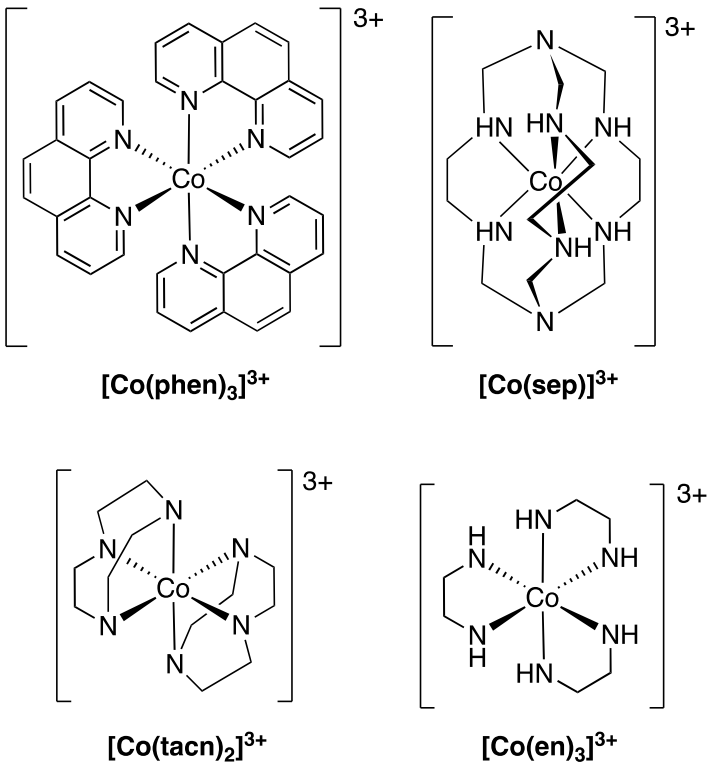

Figure S20. Test set for evaluating the accuracy of the computational methodology.

Table S5. Calculated and experimental reduction potentials for the test set in Figure S20. All values are reported in V vs. SCE, and were calculated/measured in water with the exception of $[Co(DIM)Br_2]^+$ which was determined in acetonitrile.

Complex	E^0 (calc)	E^0 (expt)	Δ
$[Co(sep)]^{3+}$	-0.53	-0.54[43]	0.01
$[Co(phen)_3]^{3+}$	0.23	0.14[44]	0.09
$[Co(en)_3]^{3+}$	-0.21	-0.46[45]	0.25
$[Co(tacn)_2]^{3+}$	-0.47	-0.62[46]	0.15
$[Co(DIM)Br_2]^+$	-0.15	-0.03	-0.12

The chosen complexes have reduction potentials that vary from -0.62 to 0.14. For every system but $[Co(en)_3]^{3+}$ the computational methodology was able to successfully match the calculated reduction potential within 0.2 V. Even $[Co(en)_3]^{3+}$, which had the largest error, only deviated by 0.25 V. The methodology was able to predict the reduction potentials of the test set with a mean signed error of 0.08 V and a mean unsigned error of 0.13 V. This is an excellent agreement, and likely as accurate as can be expect from the combination of DFT and implicit solvation models. Interestingly, these results were dramatically worse when the default PCM solvent model in Gaussian 09 was used (IEF-PCM). While this data is not presented here, for several complexes the calculated redox potentials with the IEF-PCM were ~1 V more positive than the SMD values. While the source of this error is currently unclear, any researchers attempting to calculate Co electrochemistry with DFT should be aware of this problem.

Note that the reduction potentials are systematically calculated as being too positive for the tricationic test set in Figure S20. However, the reduction potential for the more electron rich

$[Co(DIM)Br_2]^+$ is calculated as being too negative by 0.12 V. While this is an acceptable error, it is important to realize that as these complexes become more electron-rich, the error may continue to be exacerbated, and as such it is expected that that the error in calculated reduction potentials will be worse for the second reductions when compared to the first reductions. Furthermore, these calculations are representative of the methodology's ability to accurately match metal-based reductions, and it was not clear *a priori* whether this error would be smaller or larger for ligand-based reductions.

Ideally this would be evaluated by calculating the second, ligand-based reduction potential of $[Co(DIM)Br_2]^+$ as it was determined experimentally to be -0.90 V vs. SCE. As mentioned in the main text however this was not possible to do, as any attempt to optimize the structure of the direduced complex, $[Co(DIM)Br_2]^-$, resulted in dissociation of a bromide ligand. This is an unfortunate flaw in the computational methodology which suggests that it exaggerates ligand dissociation/bond-weakening in solution and that lack of a computationally determined minimum should not then be taken as proof that a given complex does not exist as a stable minimum in solution.

Despite this, an attempt was still made to computationally estimate the second reduction potential. A "window" for the reduction potential can be determined by considering first the monobromo Co(II) complex $[Co(DIM)Br]^+$, which did not undergo ligand dissociation upon reduction and its reduction potential was calculated as -1.38 V vs. SCE. It is reasonable to expect that neutral $Co(DIM)Br_2$ will not be reduced at a potential more positive than $[Co(DIM)Br]^+$, and this provides an upper bound for the window. In addition, $[Co(DIM)Br_2]^-$ was optimized in acetonitrile but the Co−Br bonds were frozen at their lengths in the optimized $Co(DIM)Br_2$ complex. As some degree of bond lengthening will undoubtedly occur upon reduction, the

calculated energy of this constrained structure should be higher than what the true complex should be. A reduction potential determined using this structure therefore should be too negative, and provide the lower bound of the window. Using this structure a potential of -1.76 V was calculated. This analysis leads to the conclusion that the present methodology would predict a potential between -1.38 V and -1.76 V, a range that is much more negative than the measured potential of -0.90 V. While some argument could be made that the constrained structure used to estimate $[Co(DIM)Br_2]^-$ may be over-exaggerating how negative this reduction potential could be, it is much harder to rationalize how the calculated reduction of the monobromo would not be a true upper bound, and -1.38 V is already far too negative compared to experiment.

The error in the calculated reduction potential of $Co(DIM)Br_2$ likely arises from two sources: one is that the methodology is not able to predict ligand-centered reductions as well as it can metal-based reductions. Recall that it was possible to accurately reproduce the metal-centered reduction of $[Co(DIM)Br_2]^+$ and other Co(III) complexes. The second source of error is that this reduction is occurring on a much more electron rich complex than the other models in the test set going from a neutral complex to an anionic one, in addition to possessing two anionic ligands. Although this error is certainly disappointing, these results can be applied usefully to the rest of the data set. First, the formally Co(III) to Co(II) reduction potentials of the Co(DIM) complexes considered in this study were likely determined with good accuracy, as the dramatic error only appeared for the second reduction. Second, we can assume that calculated formally Co(II) to Co(I) reductions are more negative than they should be. Moreover, the more anionic the ligand becomes, the greater the error.

Additional Discussion on the Computational Prediction of Active Species Formation

The method benchmarking analysis performed above offers additional insight into the accuracy of our computational predictions in Figure 5, with the data now being more consistent with experiment. The reduction of $[Co(DIM)]^{2+}$ was calculated at -1.20 V, which is reasonably similar to the observed peak potential, but still too negative. This is especially true considering that it should be close in value to the calculated first reductions of the complexes in Figure 5, if not more positive (resulting in two-electron chemistry and only one electrochemical signal). Given the error for the calculated metal-centered reduction of the dibromo complex, it can be expected that the ligand-based reduction of $[Co(DIM)]^{2+}$ should also be too negative which is exactly what was observed. This error is likely less than what is observed for the dibromo complex, however, as $[Co(DIM)]^{2+}$ is dicationic instead of neutral and probably less susceptible to error.

A less clear case is the reduction of $[Co(DIM)(OH_2)(OH)]^{2+}$ which was calculated at -0.97 V vs. SCE. As discussed in the previous section, this was a ligand-centered reduction (the metal-centered reduction always lead to ligand loss), one of the rare cases where it was possible to locate a Co(III)-DIM(-I) complex. Being a ligand-centered reduction, it could again be assumed that it will be calculated as too negative. However, Co(III)-DIM(-I) is less electron-rich than $Co(DIM)Br_2$ (another instance of dication vs. neutral) so depending on which of these features is more crucial may dictate how accurate this potential is. Overall then the benchmarking here shows that the computational methodology does have its flaws, but that the results obtained support the conclusions and assignments for the speciation relevant to the electrochemistry and catalysis presented in the manuscript.

Calculated Square Schemes

The following figures show the calculated square schemes that were used to determine the complex speciation and relevant electrochemical pathways. For each scheme, the horizontal pathways correspond to one-electron reductions and the number reported is the calculated reduction potential vs. SCE in V. The vertical pathways correspond to ligand loss/binding and the number reported is the calculated ΔG_{sol} in kcal/mol. Any molecules in grey could not be optimized due to ligand dissociation. To conserve space, the DIM ligand is represented in a very abbreviated form.

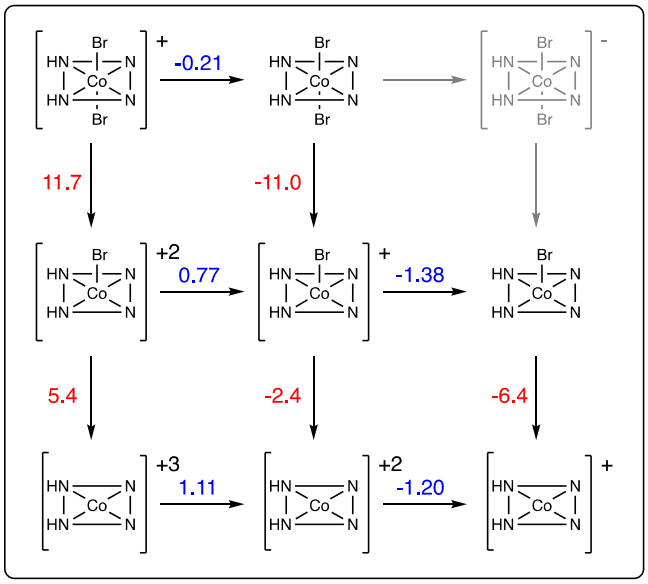

Figure S21. Calculated square scheme showing investigated electrochemical pathways for $[Co(DIM)Br_2]^+$.

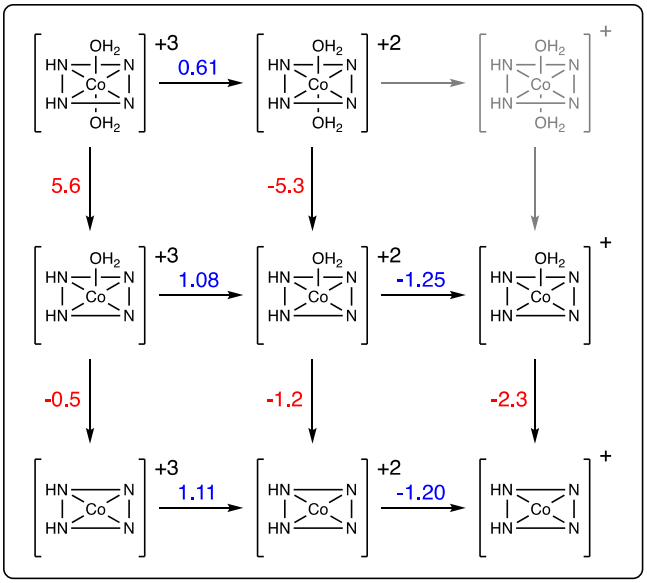

Figure S22. Calculated square scheme showing investigated electrochemical pathways for $[Co(DIM)(OH_2)_2]^{+3}$.

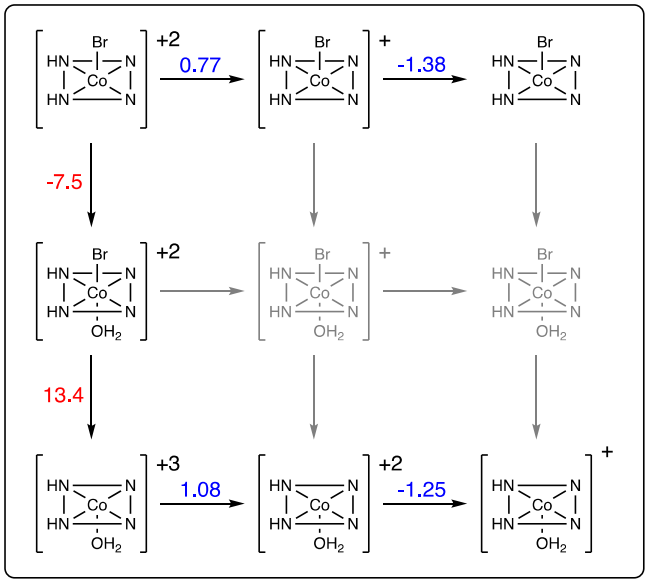

Figure S23. Calculated square scheme showing investigated electrochemical pathways for $[Co(DIM)(OH_2)Br]^{+2}$.

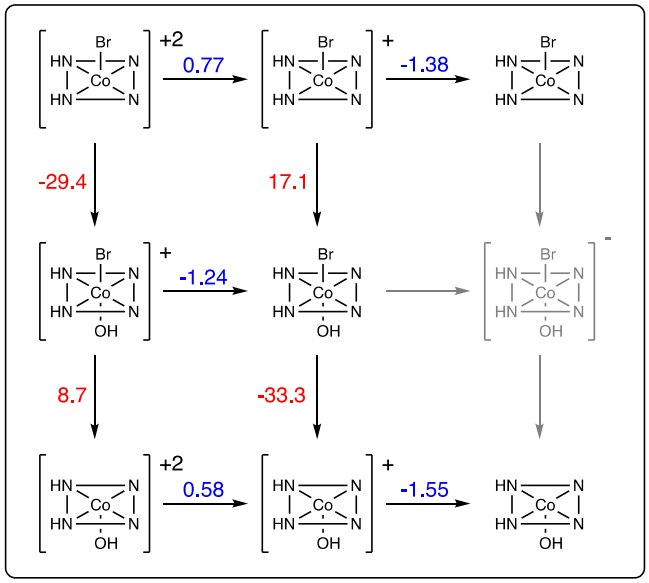

Figure S24. Calculated square scheme showing investigated electrochemical pathways for $[Co(DIM)(OH)Br]^{+}$.

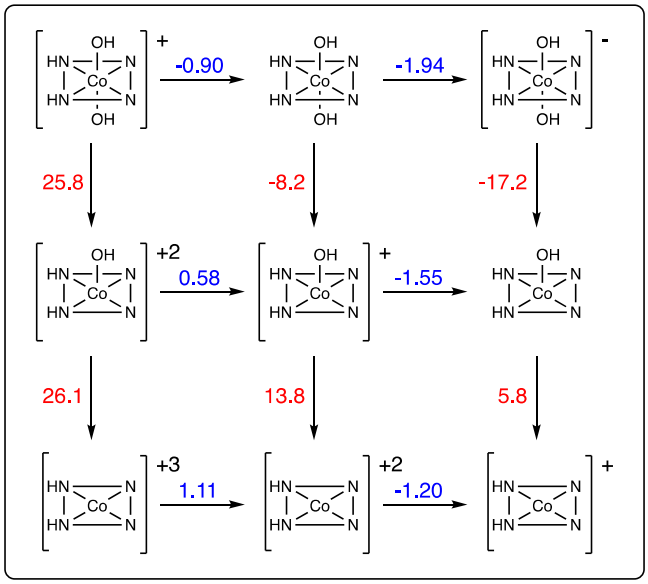

Figure S25. Calculated square scheme showing investigated electrochemical pathways for $[Co(DIM)(OH)_2]^{+}$.

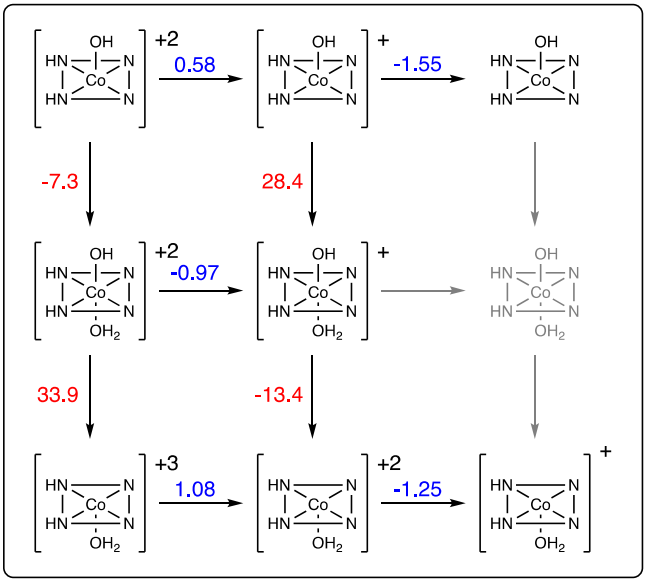

Figure S26. Calculated square scheme showing investigated electrochemical pathways for $[Co(DIM)(OH_2)(OH)]^{2+}$.

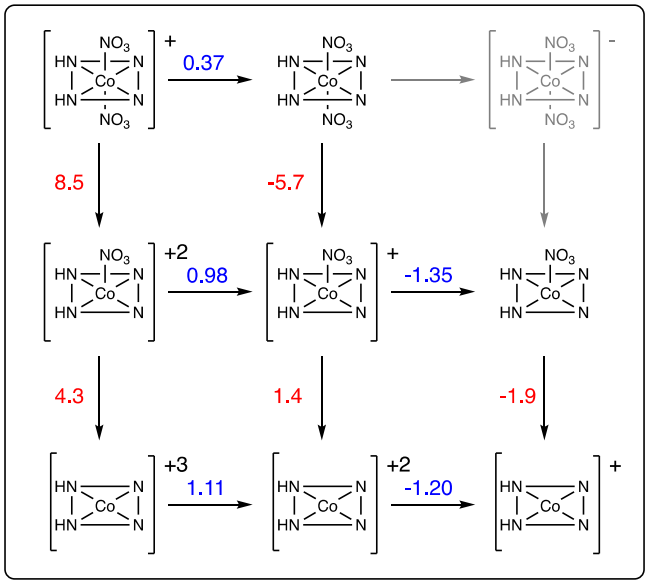

Figure S27. Calculated square scheme showing investigated electrochemical pathways for $[Co(DIM)(NO_3)_2]^{+}$.

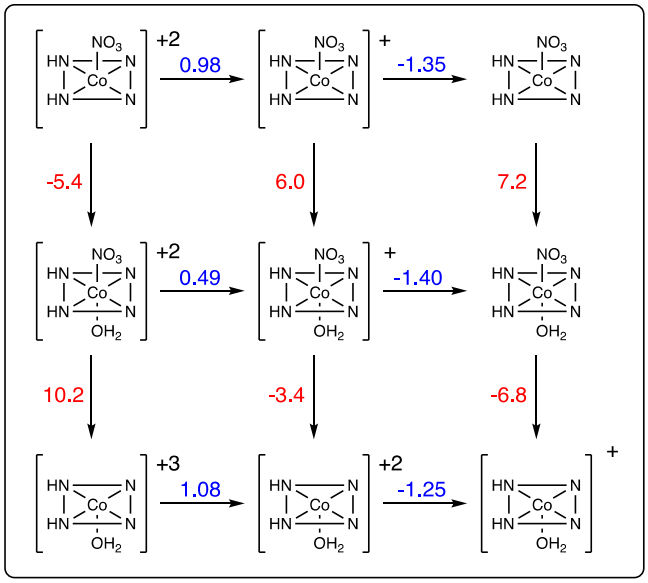

Figure S28. Calculated square scheme showing investigated electrochemical pathways for $[Co(DIM)(OH_2)(NO_3)]^{2+}$.

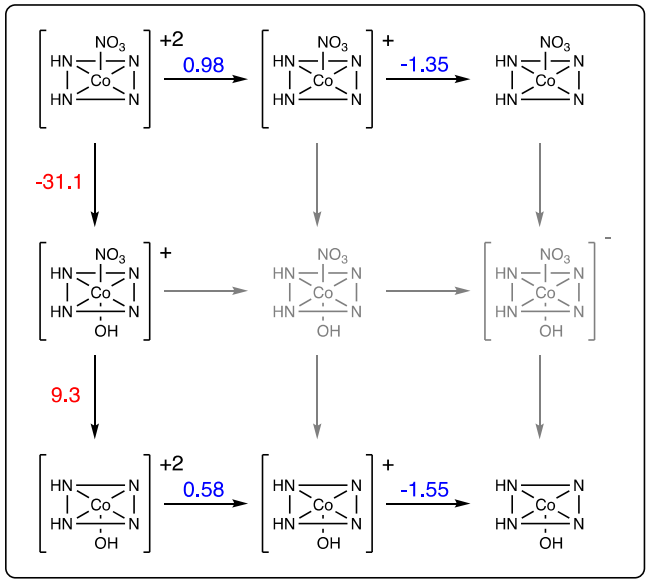

Figure S29. Calculated square scheme showing investigated electrochemical pathways for $[Co(DIM)(OH)(NO_3)]^{+}$.

Electronic Structure Issues Relevant to the Mechanistic Analysis

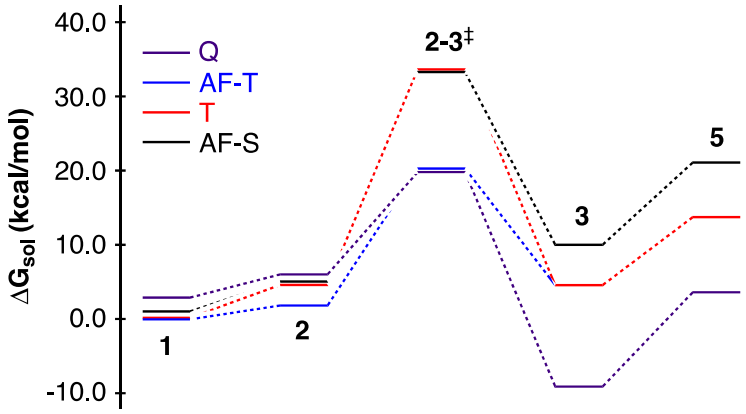

Figure S30. Reaction coordinate diagram for the "monodentate" nitrate reduction pathway shown for all examined spin states. Note that for the formally Co(III) species (**3** and **5**) the "AF" designations no longer apply as the ligand is no longer reduced.

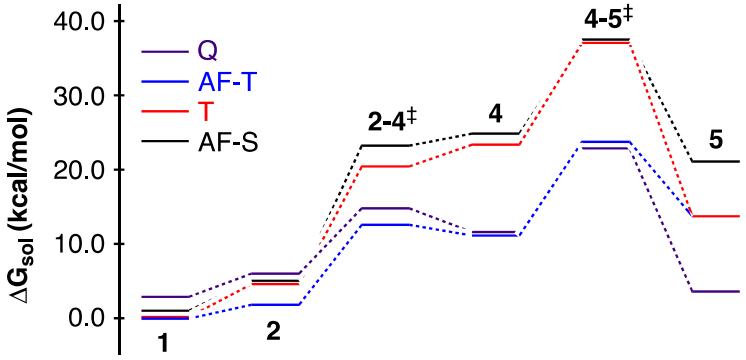

Figure S31. Reaction coordinate diagram for the "bidentate" nitrate reduction pathway shown for all examined spin states. Note that for the formally Co(III) species (**5**) the "AF" designation no longer applies as the ligand is no longer reduced.

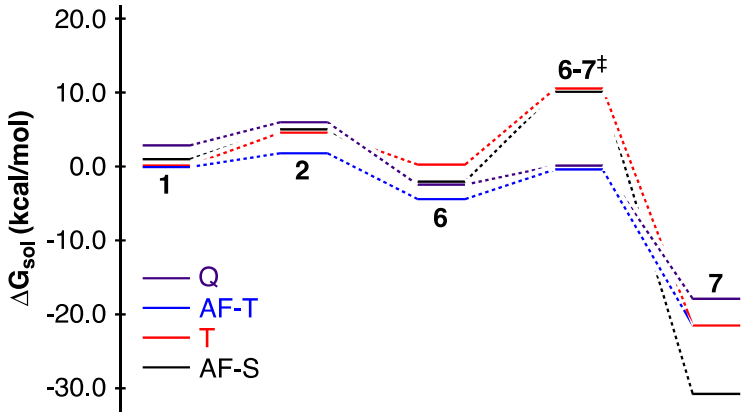

Figure S32. Reaction coordinate diagram for the "proton-assisted" nitrate reduction pathway shown for all examined spin states. Note that for the formally Co(III) species (**7**) the "AF" designation no longer applies as the ligand is no longer reduced.

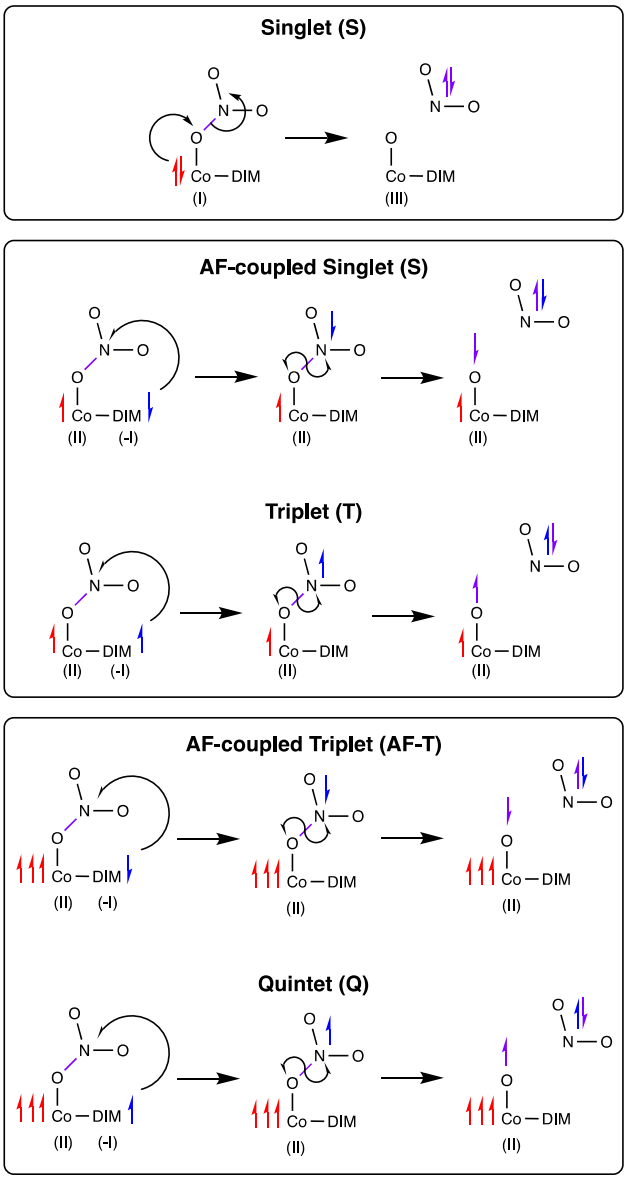

Figure S33. Schematic of electron transfer for different electronic states of $[Co(DIM)(NO_3)]^0$.

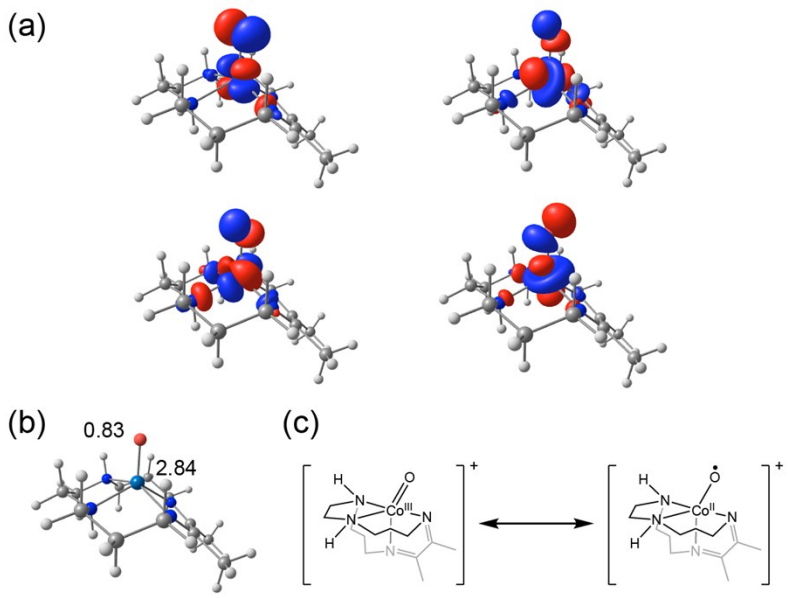

Figure S34. Electronic structure of **3** in the quintet state. **(**a) Singly occupied NOs (isovalue = 0.05 e/Å^3). Note the large amount of oxygen character in the π* orbital in the upper left. (b) Calculated Mulliken spin on the oxygen and Co atoms. (c) Simplistic scheme showing how the electronic structure of **3** can be described in terms of resonance structures and formal oxidation states.

Substrate Selectivity and Catalyst Inhibition

While electrocatalytic nitrate reduction by $[Co(DIM)Br_2]^+$ is completely inhibited by common anions, including $H_2PO_4^-$ and HCO_3^-, other anions such as OTf^- and SO_4^{2-} do not inhibit catalysis. DFT calculations showed that HCO_3^- and $H_2PO_4^-$ binding energies to various Co(DIM) complexes are stronger (more negative) than nitrate, while the binding energy of OTf^- is weaker (Table S6). This is especially true for Co(III), but less dramatic for the formally Co(I) species. The strong binding energies of these anions to the catalyst could potentially prevent nitrate from binding and undergoing reduction. These computational results agree with the experimental data with the exception of the sulfate binding energy, which is the strongest in all cases. The protonation state of the anions was chosen for weakly acidic conditions (~4-6), which results in sulfate being the

only dianion, and hence electrostatically it will have the strongest binding energy with the Co ion. That sulfate is calculated to bind the strongest either means that there is some other mitigating factor that prevents sulfate from inhibiting the reaction (perhaps the interaction of sulfate with water for example), or that the mechanism for inhibition by the other anions is not related to their ability to bind to Co more strongly than nitrate. Further investigation of the reaction mechanism will be needed to clarify this.

Table S6. Calculated ligand binding free energies of common anions to Co(DIM) catalyst at pH 7 in kcal/mol.

ΔG (kcal/mol)		$Co(DIM)^{III}L$	$Co(DIM)^{III}L_2$	$Co(DIM)^{III}(OH)L$	$Co(DIM)^{I}L$
L	NO_3^-	-4.3	-8.5	-9.3	1.8
	HCO_3^-	-9.5	-15.4	-14.3	0.5
	$H_2PO_4^-$	-10.7	-14.0	-14.2	-0.9
	SO_4^{2-}	-15.3	-13.8	-16.2	-2.1
	OTf^-	-1.6	-5.4	-8.7	3.3

Calculated Energies

Table S7. Electronic energies (E), zero-point energies (ZPE), entropic corrections to free energies (−TS), enthalpies (H), and solvated Gibbs free energies (G_{sol}) calculated with DFT. Solvated free energies not adjusted for concentration are listed as G′. All optimizations were done with the SMD correction for solvent (water unless specified otherwise), hence E contains the solvation effects. The temperature (T) was set to 298.15 K, and the pressure to 1 atm. All values are reported in kcal/mol. The concentration of all species is considered to be 1 M with the exception of water, which is treated as 55.5 M.

Complex	E	ZPE	-TΔS	H	G_{sol}	G'
$[Co(DIM)Br_2]^+$ singlet	-1048410.42	234.94	-43.73	-1048162.04	-1048203.87	-1048205.77
$[Co(DIM)Br_2]^+$ singlet Optimized in acetonitrile	-1048419.94	234.84	-43.66	-1048171.65	-1048213.42	-1048215.31
$[Co(DIM)Br_2]^+$ triplet	-1048396.34	233.85	-46.18	-1048148.56	-1048192.84	-1048194.74
$[Co(DIM)Br_2]$ doublet	-1048505.78	233.33	-46.84	-1048258.37	-1048303.31	-1048305.21
$[Co(DIM)Br_2]$ doublet Optimized in acetonitrile	-1048515.62	232.88	-47.64	-1048268.49	-1048314.23	-1048316.13
$[Co(DIM)Br_2]$ quartet	-1048502.80	231.55	-48.17	-1048256.74	-1048303.02	-1048304.92
$[Co(DIM)Br]^{2+}$ singlet	-786648.96	234.22	-40.71	-786402.53	-786441.34	-786443.24
$[Co(DIM)Br]^{2+}$ triplet	-786649.70	234.05	-41.36	-786403.38	-786442.85	-786444.75
$[Co(DIM)Br]^{2+}$ quintet	-786633.96	232.57	-43.60	-786388.65	-786430.35	-786432.25
$[Co(DIM)Br]^+$ doublet	-786767.60	233.44	-41.72	-786521.73	-786561.55	-786563.45
$[Co(DIM)Br]^+$ quartet	-786766.93	231.70	-44.72	-786522.14	-786564.96	-786566.86
[Co(DIM)Br] AF-singlet	-786836.68	231.47	-41.98	-786592.57	-786632.66	-786634.55
[Co(DIM)Br] AF-triplet	-786838.61	230.18	-44.08	-786595.30	-786637.48	-786639.38
[Co(DIM)Br] quintet	-786832.51	229.76	-44.60	-786589.51	-786632.22	-786634.11
$[Co(DIM)]^{3+}$ singlet	-524880.13	233.16	-38.70	-524635.79	-524672.59	-524674.49
$[Co(DIM)]^{3+}$ triplet	-524894.16	232.78	-39.92	-524650.11	-524688.13	-524690.03
$[Co(DIM)]^{3+}$ quintet	-524881.23	230.95	-40.04	-524638.69	-524676.83	-524678.73
$[Co(DIM)]^{2+}$ quartet	-525021.39	230.66	-41.05	-524778.84	-524817.99	-524819.89
$[Co(DIM)]^{2+}$ doublet	-525024.60	232.74	-39.26	-524780.57	-524817.94	-524819.84
$[Co(DIM)]^+$ singlet	-525099.03	230.94	-38.80	-524856.66	-524893.56	-524895.46
$[Co(DIM)]^+$ triplet	-525099.63	231.09	-39.21	-524857.18	-524894.48	-524896.38
$[Co(DIM)]^+$ AF-triplet	-525097.91	229.92	-40.19	-524856.27	-524894.56	-524896.46
$[Co(DIM)]^+$ quintet	-525094.47	229.41	-40.37	-524853.29	-524891.77	-524893.66
$[Co(DIM)(H_2O)_2]^{3+}$ singlet	-620897.10	268.56	-41.65	-620615.39	-620655.14	-620657.04
$[Co(DIM)(H_2O)_2]^{3+}$ triplet	-620887.20	266.99	-43.72	-620606.34	-620648.16	-620650.06
$[Co(DIM)(H_2O)_2]^{2+}$ doublet	-621010.27	265.31	-44.48	-620730.68	-620773.26	-620775.16
$[Co(DIM)(H_2O)_2]^{2+}$ quartet	-621006.63	262.83	-46.55	-620728.77	-620773.42	-620775.32
$[Co(DIM)(H_2O)]^{3+}$ singlet	-572886.39	250.92	-40.12	-572623.22	-572661.45	-572663.34
$[Co(DIM)(H_2O)]^{3+}$ triplet	-572891.61	249.83	-41.22	-572629.27	-572668.59	-572670.48
$[Co(DIM)(H_2O)]^{3+}$ quintet	-572873.40	248.01	-42.60	-572612.39	-572653.09	-572654.99
$[Co(DIM)(H_2O)]^{2+}$ doublet	-573018.20	248.95	-41.82	-572756.46	-572796.38	-572798.28
$[Co(DIM)(H_2O)]^{2+}$ quartet	-573017.05	247.28	-42.76	-572756.91	-572797.78	-572799.67
$[Co(DIM)(H_2O)]^+$ triplet	-573090.93	246.96	-42.24	-572830.99	-572871.33	-572873.23
$[Co(DIM)(H_2O)]^+$ AF-singlet	-573091.15	247.16	-41.49	-572831.04	-572870.63	-572872.53
$[Co(DIM)(H_2O)]^+$ AF-triplet	-573090.51	245.50	-43.51	-572831.57	-572873.19	-572875.09
$[Co(DIM)(H_2O)]^+$ quintet	-573085.72	245.20	-43.51	-572827.10	-572868.70	-572870.60
$[Co(DIM)(H_2O)Br]^{2+}$ singlet	-834655.04	251.40	-43.00	-834390.19	-834431.29	-834433.19
$[Co(DIM)(H_2O)Br]^{2+}$ triplet	-834643.14	250.15	-44.86	-834379.06	-834422.01	-834423.91
$[Co(DIM)(OH)Br]^+$ singlet	-834368.14	242.78	-42.50	-834112.08	-834152.69	-834154.58

$[Co(DIM)(OH)Br]^{+}$ triplet	-834351.61	241.73	-44.46	-834096.21	-834138.77	-834140.67
[Co(DIM)(OH)Br] doublet	-834440.50	240.50	-43.77	-834186.41	-834228.28	-834230.18
[Co(DIM)(OH)Br] doublet	-834451.59	240.42	-45.91	-834197.14	-834241.15	-834243.05
$[Co(DIM)(OH)]^{2+}$ singlet	-572609.75	241.69	-40.45	-572355.74	-572394.29	-572396.19
$[Co(DIM)(OH)]^{2+}$ triplet	-572609.71	241.83	-40.83	-572355.70	-572394.63	-572396.53
$[Co(DIM)(OH)]^{2+}$ quintet	-572602.32	240.11	-42.41	-572349.51	-572390.03	-572391.92
$[Co(DIM)(OH)]^{+}$ quartet	-572722.41	238.59	-43.40	-572470.69	-572512.20	-572514.09
$[Co(DIM)(OH)]^{+}$ doublet	-572714.45	240.19	-41.49	-572461.65	-572501.24	-572503.14
[Co(DIM)(OH)] AF-singlet	-572783.80	238.49	-40.80	-572532.69	-572571.59	-572573.49
[Co(DIM)(OH)] triplet	-572780.97	237.98	-41.74	-572530.25	-572570.10	-572571.99
[Co(DIM)(OH)] AF-triplet	-572789.92	237.31	-43.23	-572539.46	-572580.79	-572582.69
[Co(DIM)(OH)] quintet	-572784.37	236.68	-43.86	-572534.37	-572576.33	-572578.23
$[Co(DIM)(OH)_2]^{+}$ singlet	-620324.70	250.38	-41.58	-620061.13	-620100.81	-620102.70
$[Co(DIM)(OH)_2]^{+}$ triplet	-620307.41	248.67	-43.23	-620045.13	-620086.46	-620088.36
$[Co(DIM)(OH)_2]$ doublet	-620396.93	248.17	-42.26	-620135.39	-620175.75	-620177.64
$[Co(DIM)(OH)_2]$ doublet	-620395.10	246.91	-44.34	-620134.06	-620176.51	-620178.41
$[Co(DIM)(OH)_2]$ quartet	-620400.95	245.58	-45.37	-620140.95	-620184.42	-620186.32
$[Co(DIM)(OH)_2]^{-}$ singlet	-620452.63	246.73	-40.71	-620192.87	-620231.68	-620233.58
$[Co(DIM)(OH)_2]^{-}$ triplet	-620457.51	243.60	-44.71	-620199.54	-620242.36	-620244.26
$[Co(DIM)(OH)_2]^{-}$ quintet	-620458.70	243.59	-45.27	-620200.64	-620244.01	-620245.90
$[Co(DIM)(OH)(OH_2)]^{2+}$ singlet	-620615.10	258.98	-42.09	-620342.72	-620382.92	-620384.82
$[Co(DIM)(OH)(OH_2)]^{+}$ doublet	-620694.74	257.15	-42.60	-620424.07	-620464.78	-620466.68
$[Co(DIM)(NO_3)_2]^{+}$ singlet	-877038.21	255.03	-49.47	-876767.20	-876814.78	-876816.67
$[Co(DIM)(NO_3)_2]^{+}$ triplet	-877027.42	253.35	-51.56	-876757.51	-876807.17	-876809.07
$[Co(DIM)(NO_3)_2]^{+}$ quintet	-877004.54	251.45	-52.51	-876736.07	-876786.69	-876788.58
$[Co(DIM)(NO_3)_2]$ doublet	-877145.82	252.48	-53.17	-876876.29	-876927.56	-876929.46
$[Co(DIM)(NO_3)]^{2+}$ singlet	-700958.71	244.09	-43.83	-700701.03	-700742.96	-700744.86
$[Co(DIM)(NO_3)]^{2+}$ triplet	-700962.41	242.95	-45.76	-700705.49	-700749.36	-700751.25
$[Co(DIM)(NO_3)]^{2+}$ quintet	-700946.77	242.12	-46.64	-700690.43	-700735.17	-700737.06
$[Co(DIM)(NO_3)]^{2+}$ singlet bidentate	-700968.07	245.97	-41.08	-700709.31	-700748.49	-700750.39
$[Co(DIM)(NO_3)]^{2+}$ triplet bidentate	-700957.67	243.46	-44.81	-700700.42	-700743.33	-700745.23
$[Co(DIM)(NO_3)]^{2+}$ quintet bidentate	-700942.80	242.09	-46.54	-700686.45	-700731.09	-700732.99
$[Co(DIM)(NO_3)]^{+}$ quartet	-701086.35	241.16	-47.55	-700830.67	-700876.32	-700878.22
$[Co(DIM)(NO_3)]^{+}$ doublet	-701086.24	242.32	-46.48	-700829.69	-700874.27	-700876.17
$[Co(DIM)(NO_3)]$ triplet	-701157.87	241.05	-46.06	-700902.65	-700946.82	-700948.72
$[Co(DIM)(NO_3)]$ AF-triplet	-701158.40	239.64	-47.31	-700904.15	-700949.57	-700951.46
$[Co(DIM)(NO_3)]$ quintet	-701153.05	239.21	-48.21	-700899.13	-700945.44	-700947.34
$[Co(DIM)(NO_3)]$ AF-singlet	-701158.19	241.03	-45.37	-700902.96	-700946.44	-700948.33
$[Co(DIM)(NO_3)(H_2O))]^{2+}$ triplet	-748957.10	260.14	-48.08	-748681.66	-748727.85	-748729.75
$[Co(DIM)(NO_3)(H_2O)]^{2+}$ singlet	-748967.85	261.21	-45.69	-748691.90	-748735.69	-748737.59
$[Co(DIM)(NO_3)(H_2O))]^{2+}$	-748938.57	258.83	-47.11	-748664.50	-748709.71	-748711.60

quintet						
$[Co(DIM)(NO_3)(H_2O)]^+$ doublet	-749078.75	258.71	-48.83	-748804.33	-748851.26	-748853.16
$[Co(DIM)(NO_3)(H_2O)]^+$ quartet	-749074.26	257.46	-49.41	-748800.89	-748848.40	-748850.29
$[Co(DIM)(NO_3)(H_2O)]$ triplet	-749148.49	256.68	-49.34	-748875.86	-748923.30	-748925.20
$[Co(DIM)(NO_3)(OH)]^+$ triplet	-748670.19	251.43	-46.92	-748403.71	-748448.73	-748450.63
$[Co(DIM)(NO_3)(OH)]^+$ singlet	-748683.50	252.34	-46.39	-748416.34	-748460.83	-748462.73
Nitrite	-128847.36	4.91	-17.30	-128840.02	-128855.42	-128857.32
Bromide	-261741.10	0.00	-11.63	-261739.61	-261749.35	-261751.25
Nitrate	-176051.56	8.75	-18.58	-176040.23	-176056.92	-176058.82
Water	-47986.87	13.14	-13.87	-47971.36	-47980.95	-47985.23
Hydroxide	-47677.25	5.18	-12.28	-47670.00	-47680.39	-47682.29
Bicarbonate	-166079.74	16.62	-18.96	-166060.32	-166075.00	-166079.28
Dihydrogen phosphate	-404035.99	22.65	-22.62	-404009.08	-404029.80	-404031.70
Sulfate	-438939.41	9.48	-20.46	-438926.76	-438945.32	-438947.22
Triflate	-603553.82	16.94	-25.55	-603531.77	-603553.04	-603557.32
$[Co(DIM)(HCO_3)]^{2+}$ singlet	-690994.36	251.91	-43.75	-690728.78	-690770.63	-690772.53
$[Co(DIM)(HCO_3)]^{2+}$ triplet	-690996.85	250.51	-44.22	-690732.74	-690775.07	-690776.96
$[Co(DIM)(HCO_3)]^{2+}$ quintet	-690983.44	250.31	-45.85	-690719.02	-690762.97	-690764.87
$[Co(DIM)(HCO_3)]^{2+}$ triplet bidentate	-690989.69	251.26	-45.05	-690724.49	-690767.63	-690769.53
$[Co(DIM)(HCO_3)]$ singlet	-691173.93	249.71	-44.43	-690910.29	-690952.83	-690954.72
$[Co(DIM)(HCO_3)]$ AF-singlet	-691187.58	248.78	-45.32	-690924.52	-690967.94	-690969.83
$[Co(DIM)(HCO_3)]$ triplet	-691186.76	248.92	-45.52	-690923.68	-690967.30	-690969.20
$[Co(DIM)(HCO_3)]$ AF-triplet	-691188.46	247.51	-47.00	-690926.29	-690971.39	-690973.28
$[Co(DIM)(HCO_3)]$ quintet	-691182.87	246.65	-47.98	-690921.31	-690967.39	-690969.28
$[Co(DIM)(HCO_3)_2]^+$ singlet	-857106.39	270.16	-49.94	-856819.84	-856867.89	-856869.79
$[Co(DIM)(HCO_3)_2]^+$ triplet	-857093.09	267.99	-53.36	-856807.90	-856859.36	-856861.26
$[Co(DIM)(HCO_3)_2]^+$ quintet	-857073.43	266.98	-53.20	-856789.13	-856840.43	-856842.32
$[Co(DIM)(HCO_3)(OH)]^+$ singlet	-738716.93	260.07	-46.33	-738441.92	-738486.36	-738488.26
$[Co(DIM)(HCO_3)(OH)]^+$ triplet	-738697.15	258.57	-47.35	-738423.33	-738468.78	-738470.68
$[Co(DIM)(HCO_3)(OH)]^+$ quintet	-738689.04	257.65	-48.57	-738415.90	-738462.58	-738464.47
$[Co(DIM)(HCO_3)(H_2O)]^{2+}$ singlet	-739002.52	269.05	-45.80	-738718.63	-738762.54	-738764.44
$[Co(DIM)(HCO_3)(H_2O)]^{2+}$ triplet	-738991.08	267.81	-47.30	-738707.97	-738753.37	-738755.27
$[Co(DIM)(HCO_3)(H_2O)]^{2+}$ quintet	-738971.21	266.11	-48.77	-738689.36	-738736.23	-738738.13
$[Co(DIM)(H_2PO_4)]^{2+}$ singlet	-928951.02	258.29	-46.59	-928677.63	-928722.33	-928724.22
$[Co(DIM)(H_2PO_4)]^{2+}$ triplet	-928954.72	257.16	-48.47	-928682.10	-928728.67	-928730.57
$[Co(DIM)(H_2PO_4)]^{2+}$ quintet	-928941.65	256.64	-48.86	-928669.45	-928716.42	-928718.31
$[Co(DIM)(H_2PO_4)]$ singlet	-929130.95	255.90	-47.66	-928859.61	-928905.37	-928907.27
$[Co(DIM)(H_2PO_4)]$ AF-singlet	-929145.47	255.18	-48.14	-928874.61	-928920.85	-928922.75
$[Co(DIM)(H_2PO_4)]$ triplet	-929144.85	254.84	-49.15	-928874.22	-928921.47	-928923.37
$[Co(DIM)(H_2PO_4)]$ AF-triplet	-929146.33	253.80	-50.81	-928876.25	-928925.16	-928927.06

[Co(DIM)(H_2PO_4)] quintet	-929141.82	253.44	-50.36	-928872.21	-928920.67	-928922.57
[Co(DIM)(H_2PO_4)$_2$]$^+$ singlet	-1333022.30	283.56	-54.58	-1332719.81	-1332772.49	-1332774.38
[Co(DIM)(H_2PO_4)$_2$]$^+$ triplet	-1333005.94	281.37	-57.76	-1332704.80	-1332760.66	-1332762.56
[Co(DIM)(H_2PO_4)$_2$]$^+$ quintet	-1332991.62	280.03	-58.57	-1332691.60	-1332748.27	-1332750.17
[Co(DIM)(H_2PO_4)(OH)]$^+$ singlet	-976674.18	266.63	-49.30	-976391.20	-976438.60	-976440.50
[Co(DIM)(H_2PO_4)(OH)]$^+$ triplet	-976655.31	265.19	-50.08	-976373.52	-976421.70	-976423.60
[Co(DIM)(H_2PO_4)(OH)]$^+$ quintet	-976647.64	264.40	-50.88	-976366.47	-976415.45	-976417.34
[Co(DIM)(H_2PO_4)(H_2O)]$^{2+}$ singlet	-976959.08	275.49	-49.06	-976667.27	-976714.44	-976716.33
[Co(DIM)(H_2PO_4)(H_2O)]$^{2+}$ triplet	-976948.65	274.08	-50.93	-976657.75	-976706.79	-976708.69
[Co(DIM)(H_2PO_4)(H_2O)]$^{2+}$ quintet	-976930.15	272.71	-51.79	-976640.39	-976690.29	-976692.18
[Co(DIM)(SO_4)]$^+$ singlet	-963858.43	244.18	-45.81	-963599.83	-963643.75	-963645.64
[Co(DIM)(SO_4)]$^+$ triplet	-963861.33	243.41	-47.39	-963603.27	-963648.76	-963650.66
[Co(DIM)(SO_4)]$^+$ quintet	-963849.68	242.97	-47.58	-963591.94	-963637.62	-963639.52
[Co(DIM)(SO_4)]$^-$ singlet	-964034.19	242.29	-45.45	-963777.45	-963821.00	-963822.90
[Co(DIM)(SO_4)]$^-$ AF-singlet	-964048.05	241.58	-46.13	-963791.74	-963835.97	-963837.87
[Co(DIM)(SO_4)]$^-$ triplet	-964047.19	241.44	-46.71	-963791.04	-963835.85	-963837.75
[Co(DIM)(SO_4)]$^-$ AF-triplet	-964049.64	240.21	-49.67	-963794.11	-963841.89	-963843.79
[Co(DIM)(SO_4)]$^-$ quintet	-964043.63	239.89	-48.74	-963788.50	-963835.34	-963837.24
[Co(DIM)(SO_4)$_2$]$^-$ singlet	-1402829.51	255.33	-53.24	-1402556.54	-1402607.88	-1402609.78
[Co(DIM)(SO_4)$_2$]$^-$ triplet	-1402818.88	253.89	-54.74	-1402546.94	-1402599.78	-1402601.67
[Co(DIM)(SO_4)$_2$]$^-$ quintet	-1402802.16	252.54	-55.96	-1402531.19	-1402585.25	-1402587.15
[Co(DIM)(SO_4)(OH)] singlet	-1011578.65	252.78	-47.68	-1011310.37	-1011356.15	-1011358.05
[Co(DIM)(SO_4)(OH)] triplet	-1011559.64	251.08	-48.55	-1011292.74	-1011339.39	-1011341.29
[Co(DIM)(SO_4)(OH)] quintet	-1011551.71	250.10	-50.20	-1011285.41	-1011333.71	-1011335.61
[Co(DIM)(SO_4)(H_2O)]$^+$ singlet	-1011865.03	261.47	-47.46	-1011588.03	-1011633.59	-1011635.49
[Co(DIM)(SO_4)(H_2O)]$^+$ triplet	-1011854.96	259.72	-49.55	-1011579.09	-1011626.74	-1011628.64
[Co(DIM)(SO_4)(H_2O)]$^+$ quintet	-1011838.80	259.13	-50.22	-1011563.41	-1011611.73	-1011613.63
[Co(DIM)(OTf)]$^{2+}$ singlet	-1128458.21	252.06	-49.16	-1128189.91	-1128237.17	-1128239.06
[Co(DIM)(OTf)]$^{2+}$ triplet	-1128463.84	251.20	-50.96	-1128196.09	-1128245.15	-1128247.05
[Co(DIM)(OTf)]$^{2+}$ quintet	-1128444.18	249.26	-53.65	-1128177.75	-1128229.51	-1128231.41
[Co(DIM)(OTf)] singlet	-1128648.65	250.18	-49.78	-1128382.04	-1128429.92	-1128431.81
[Co(DIM)(OTf)] AF-singlet	-1128662.60	249.48	-50.62	-1128396.47	-1128445.19	-1128447.09
[Co(DIM)(OTf)] triplet	-1128661.92	249.33	-51.55	-1128395.91	-1128445.56	-1128447.46

[Co(DIM)(OTf)] AF-triplet	-1128660.51	247.74	-52.93	-1128395.59	-1128446.62	-1128448.51
[Co(DIM)(OTf)] quintet	-1128655.95	247.52	-52.52	-1128391.29	-1128441.91	-1128443.81
$[Co(DIM)(OTf)_2]^+$ singlet	-1732039.38	270.90	-60.74	-1731747.12	-1731805.96	-1731807.86
$[Co(DIM)(OTf)_2]^+$ triplet	-1732032.42	269.43	-63.08	-1731741.08	-1731802.26	-1731804.15
$[Co(DIM)(OTf)_2]^+$ quintet	-1732007.73	267.56	-64.40	-1731717.78	-1731780.28	-1731782.18
$[Co(DIM)(OTf)(OH)]^+$ singlet	-1176186.21	260.36	-52.34	-1175908.32	-1175958.76	-1175960.66
$[Co(DIM)(OTf)(OH)]^+$ triplet	-1176176.91	259.87	-52.68	-1175899.48	-1175950.26	-1175952.16
$[Co(DIM)(OTf)(H_2O)]^{2+}$ singlet	-1176468.15	269.52	-51.06	-1176181.29	-1176230.46	-1176232.36
$[Co(DIM)(OTf)(H_2O)]^{2+}$ triplet	-1176459.58	268.23	-53.54	-1176173.45	-1176225.09	-1176226.99
$[Co(DIM)(OTf)(H_2O)]^{2+}$ quintet	-1176436.72	266.35	-53.94	-1176152.12	-1176204.16	-1176206.06
(Figure 9) 4 AF-singlet	-701139.61	240.91	-43.79	-700884.84	-700926.73	-700928.63
(Figure 9) 4 triplet	-701140.19	240.88	-44.69	-700885.40	-700928.19	-700930.09
(Figure 9) 4 AF-triplet	-701150.71	239.96	-45.67	-700896.45	-700940.22	-700942.12
(Figure 9) 4 quintet	-701148.69	239.60	-47.14	-700894.61	-700939.85	-700941.75
(Figure 9) 5 AF-singlet	-701144.55	242.01	-43.63	-700888.66	-700930.39	-700932.29
(Figure 9) 5 triplet	-701147.29	240.07	-47.08	-700892.47	-700937.65	-700939.55
(Figure 9) 5 quintet	-701157.31	239.63	-46.84	-700902.94	-700947.89	-700949.78
(Figure 9) 3 AF-singlet	-572294.82	234.31	-39.36	-572048.59	-572086.06	-572087.96
(Figure 9) 3 triplet	-572298.65	233.80	-40.65	-572052.72	-572091.48	-572093.37
(Figure 9) 3 quintet	-572311.31	233.42	-41.49	-572065.59	-572105.18	-572107.08
(Figure 9) 7 singlet	-701475.56	250.00	-43.29	-701211.63	-701253.03	-701254.93
(Figure 9) 7 triplet	-701462.52	248.28	-46.01	-701199.65	-701243.76	-701245.66
(Figure 9) 7 quintet	-701456.57	246.83	-47.29	-701194.76	-701240.15	-701242.05
(Figure 9) 6 AF-singlet	-701444.06	248.46	-45.11	-701181.27	-701224.49	-701226.38
(Figure 9) 6 triplet	-701440.31	248.23	-46.33	-701177.60	-701222.03	-701223.93
(Figure 9) 6 AF- triplet	-701443.13	246.93	-47.32	-701181.31	-701226.73	-701228.62
(Figure 9) 6 quintet	-701440.86	246.98	-47.62	-701178.99	-701224.71	-701226.61
(Figure 9) 2-4 TS AF-singlet	-701138.50	239.54	-45.27	-700884.96	-700928.33	-700930.23
(Figure 9) 2-4 TS triplet	-701140.55	239.31	-45.82	-700887.18	-700931.10	-700933.00
(Figure 9) 2-4 TS AF-triplet	-701147.07	238.34	-46.39	-700894.33	-700938.82	-700940.72
(Figure 9) 2-4 TS quintet	-701143.19	237.80	-47.77	-700890.76	-700936.63	-700938.52
(Figure 9) 4-5 TS AF-singlet	-701124.71	239.54	-44.91	-700870.99	-700914.01	-700915.90
(Figure 9) 4-5 TS triplet	-701124.91	239.68	-45.21	-700871.15	-700914.46	-700916.36
(Figure 9) 4-5 TS AF-triplet	-701135.92	238.41	-46.60	-700882.95	-700927.65	-700929.55
(Figure 9) 4-5 TS quintet	-701137.03	238.57	-46.48	-700883.99	-700928.58	-700930.48
(Figure 9) 2-3 TS AF-singlet	-701129.20	239.60	-44.60	-700875.50	-700918.20	-700920.10
(Figure 9) 2-3 TS triplet	-701128.31	239.68	-45.15	-700874.56	-700917.82	-700919.72
(Figure 9) 2-3 TS AF-triplet	-701139.24	238.38	-47.19	-700886.21	-700931.51	-700933.40
(Figure 9) 2-3 TS quintet	-701138.98	238.32	-47.46	-700886.04	-700931.60	-700933.50

(Figure 9) 6-7 TS AF-singlet	-701430.04	247.39	-45.76	-701168.25	-701212.11	-701214.00
(Figure 9) 6-7 TS triplet	-701430.51	247.74	-45.13	-701168.64	-701211.87	-701213.77
(Figure 9) 6-7 TS AF-triplet	-701439.14	246.59	-46.42	-701178.00	-701222.52	-701224.42
(Figure 9) 6-7 TS quintet	-701438.41	246.63	-46.94	-701177.24	-701222.28	-701224.18

References

1. Weatherburn, M. W., Phenol-hypochlorite reaction for determination of ammonia. *Anal. Chem.* **1967,** *39* (8), 971-974.
2. Frear, D. S.; Burrell, R. C., Spectrophotometric Method for Determining Hydroxylamine Reductase Activity in Higher Plants. *Anal. Chem.* **1955,** *27* (10), 1664-1665.
3. Jackels, S. C.; Farmery, K.; Barefield, E. K.; Rose, N. J.; Busch, D. H., Tetragonal cobalt(III) complexes containing tetradentate macrocyclic amine ligands with different degrees of unsaturation. *Inorg. Chem.* **1972,** *11* (12), 2893-2901.
4. Rountree, E. S.; McCarthy, B. D.; Eisenhart, T. T.; Dempsey, J. L., Evaluation of Homogeneous Electrocatalysts by Cyclic Voltammetry. *Inorg. Chem.* **2014,** *53* (19), 9983-10002.
5. Costentin, C.; Savéant, J. M., Multielectron, Multistep Molecular Catalysis of Electrochemical Reactions: Benchmarking of Homogeneous Catalysts. *ChemElectroChem* **2014,** *1* (7), 1226-1236.
6. Ma, L.; Li, H., Electrocatalysis of adsorbed Co-cyclam at Au electrodes for nitrate reduction in concentrated alkaline solution. *Electroanalysis* **1995,** *7* (8), 756-758.
7. Naumkin. A. V., K.-V. A., Gaarenstroom. S. W., Powell. C. J. , *X-ray Photoelectron Spectroscopy Database* National Institute of Standards and Technology (NIST), 2012.
8. Taniguchi, L.; Nakashima, N.; Yasukouchi, K., Reduction of nitrate to give hydroxylamine at a mercury electrode using cobalt(III)-and nickel(II)-cyclams as catalysts. *J. Chem. Soc., Chem. Commun.* **1986,** (24), 1814-1815.
9. Taniguchi, I.; Nakashima, N.; Matsushita, K.; Yasukouchi, K., Electrocatalytic reduction of nitrate and nitrite to hydroxylamine and ammonia using metal cyclams. *J. Electroanal. Chem. Interfacial Electrochem.* **1987,** *224* (1), 199-209.
10. Li, H. L.; Anderson, W. C.; Chambers, J. Q.; Hobbs, D. T., Electrocatalytic reduction of nitrate in sodium hydroxide solution in the presence of low-valent cobalt-cyclam species. *Inorg. Chem.* **1989,** *28* (5), 863-868.
11. Sisley, M. J.; Jordan, R. B., First Hydrolysis Constants of Hexaaquacobalt(III) and -manganese(III): Longstanding Issues Resolved. *Inorg. Chem.* **2006,** *45* (26), 10758-10763.
12. Gilson, R.; Durrant, M. C., Estimation of the pK_a values of water ligands in transition metal complexes using density functional theory with polarized continuum model solvent corrections. *Dalton Trans.* **2009,** (46), 10223-10230.
13. Hawkins, C.; Sargeson, A.; Searle, G., Acid dissociation constants of some aquo amine cobalt(III) complexes. *Aust. J. Chem.* **1964,** *17* (5), 598-600.
14. Chylewska, A.; Jacewicz, D.; Zarzeczańska, D.; Chmurzyński, L., Determination of dissociation constants for coordination compounds of Cr(III) and Co(III) using potentiometric and spectrophotometric methods. *J. Chem. Thermodyn.* **2008,** *40* (8), 1290-1294.
15. Visser, H. G.; Purcell, W.; Basson, S. S., Kinetic study of the protonations and substitutions of different cobalt(III)–nta complexes. *Transition Met. Chem.* **2002,** *27* (5), 461-468.
16. Girolami, G. S.; Rauchfuss, T. B.; Angelici, R. J., *Synthesis and Technique in Inorganic Chemistry: A Laboratory Manual*. University Science Books: 1999.
17. Feltham, R. D.; Hayter, R. G., 875. The electrolyte type of ionized complexes. *J. Chem. Soc.* **1964**, 4587-4591.

18. Becke, A. D., Density-functional exchange-energy approximation with correct asymptotic behavior. *Phys. Rev. A* **1988,** *38* (6), 3098-3100.
19. Lee, C.; Yang, W.; Parr, R. G., Development of the Colle-Salvetti correlation-energy formula into a functional of the electron density. *Phys. Rev. B* **1988,** *37* (2), 785-789.
20. Becke, A. D., Density-functional thermochemistry. III. The role of exact exchange. *J. Chem. Phys.* **1993,** *98*, 5648-5652.
21. Becke, A. D., A new mixing of Hartree–Fock and local density-functional theories. *J. Chem. Phys.* **1993,** *98* (2), 1372.
22. Grimme, S., Semiempirical GGA-type density functional constructed with a long-range dispersion correction. *J. Comput. Chem.* **2006,** *27* (15), 1787-1799.
23. Marenich, A. V.; Cramer, C. J.; Truhlar, D. G., Universal Solvation Model Based on Solute Electron Density and on a Continuum Model of the Solvent Defined by the Bulk Dielectric Constant and Atomic Surface Tensions. *J. Phys. Chem. B* **2009,** *113* (18), 6378-6396.
24. Dolg, M.; Wedig, U.; Stoll, H.; Preuss, H., Energy-adjusted ab initio pseudopotentials for the first row transition elements. *J. Chem. Phys.* **1987,** *86* (2), 866-872.
25. Martin, J. M. L.; Sundermann, A., Correlation consistent valence basis sets for use with the Stuttgart–Dresden–Bonn relativistic effective core potentials: The atoms Ga–Kr and In–Xe. *J. Chem. Phys.* **2001,** *114* (8), 3408-3420.
26. Peterson, K. A.; Figgen, D.; Goll, E.; Stoll, H.; Dolg, M., Systematically convergent basis sets with relativistic pseudopotentials. II. Small-core pseudopotentials and correlation consistent basis sets for the post-d group 16–18 elements. *J. Chem. Phys.* **2003,** *119* (21), 11113-11123.
27. Hariharan, P. C.; Pople, J. A., The influence of polarization functions on molecular orbital hydrogenation energies. *Thero. Chim. Acta* **1973,** *28* (3), 213-222.
28. Francl, M. M.; Pietro, W. J.; Hehre, W. J.; Binkley, J. S.; Gordon, M. S.; DeFrees, D. J.; Pople, J. A., Self-consistent molecular orbital methods. XXIII. A polarization-type basis set for second-row elements. *J. Chem. Phys.* **1982,** *77* (7), 3654-3665.
29. Krishnan, R.; Binkley, J. S.; Seeger, R.; Pople, J. A., Self-consistent molecular orbital methods. XX. A basis set for correlated wave functions. *J. Chem. Phys.* **1980,** *72* (1), 650-654.
30. McLean, A. D.; Chandler, G. S., Contracted Gaussian basis sets for molecular calculations. I. Second row atoms, Z=11–18. *J. Chem. Phys.* **1980,** *72* (10), 5639-5648.
31. Cramer, C. J., *Essentials of Computational Chemistry: Theories and Models.* 2nd ed.; John WIley & Sons: 2004.
32. Frisch, M. J.; Trucks, G. W.; Schlegel, H. B.; Scuseria, G. E.; Robb, M. A.; Cheeseman, J. R.; Scalmani, G.; Barone, V.; Mennucci, B.; Petersson, G. A.; Nakatsuji, H.; Caricato, M.; Li, X.; Hratchian, H. P.; Izmaylov, A. F.; Bloino, J.; Zheng, G.; Sonnenberg, J. L.; Hada, M.; Ehara, M.; Toyota, K.; Fukuda, R.; Hasegawa, J.; Ishida, M.; Nakajima, T.; Honda, Y.; Kitao, O.; Nakai, H.; Vreven, T.; Montgomery, J. A., Jr.; Peralta, J. E.; Ogliaro, F.; Bearpark, M.; Heyd, J. J.; Brothers, E.; Kudin, K. N.; Staroverov, V. N.; Kobayashi, R.; Normand, J.; Raghavachari, K.; Rendell, A.; Burant, J. C.; lyengar, S. S.; Tomasi, J.; Cossi, M.; Rega, N.; Millam, N. J.; Klene, M.; Knox, J. E.; Cross, J. B.; Bakken, V.; Adamo, C.; Jaramillo, J.; Gomperts, R.; Stratmann, R. E.; Yazyev, O.; Austin, A. J.; Cammi, R.; Pomelli, C.; Ochterski, J. W.; Martin, R. L.; Morokuma, K.; Zakrzewski, V. G.; Voth, G. A.; Salvador, P.; Dannenberg, J. J.; Dapprich, S.; Daniels, A. D.; Farkas, Ö.; Foresman, J. B.; Ortiz, J. V.; Cioslowski, J.; Fox, D. J. *Gaussian 09, Rev D.01*, Gaussian 09, revision D.01; Gaussian, Inc.: Willingford CT, 2009.

33. Kelly, C. P.; Cramer, C. J.; Truhlar, D. G., Aqueous Solvation Free Energies of Ions and Ion−Water Clusters Based on an Accurate Value for the Absolute Aqueous Solvation Free Energy of the Proton. *J. Phys. Chem. B* **2006,** *110* (32), 16066-16081.
34. Kelly, C. P.; Cramer, C. J.; Truhlar, D. G., Single-Ion Solvation Free Energies and the Normal Hydrogen Electrode Potential in Methanol, Acetonitrile, and Dimethyl Sulfoxide. *J. Phys. Chem. B* **2007,** *111* (2), 408-422.
35. Fawcett, W. R., The Ionic Work Function and its Role in Estimating Absolute Electrode Potentials. *Langmuir* **2008,** *24* (17), 9868-9875.
36. Tissandier, M. D.; Cowen, K. A.; Feng, W. Y.; Gundlach, E.; Cohen, M. H.; Earhart, A. D.; Coe, J. V.; Tuttle, T. R., The Proton's Absolute Aqueous Enthalpy and Gibbs Free Energy of Solvation from Cluster-Ion Solvation Data. *J. Phys. Chem. A* **1998,** *102* (40), 7787-7794.
37. Tissandier, M. D.; Cowen, K. A.; Feng, W. Y.; Gundlach, E.; Cohen, M. H.; Earhart, A. D.; Tuttle, T. R.; Coe, J. V., The Proton's Absolute Aqueous Enthalpy and Gibbs Free Energy of Solvation from Cluster Ion Solvation Data. *J. Phys. Chem. A* **1998,** *102* (46), 9308-9308.
38. Zhan, C.-G.; Dixon, D. A., Absolute Hydration Free Energy of the Proton from First-Principles Electronic Structure Calculations. *J. Phys. Chem. A* **2001,** *105* (51), 11534-11540.
39. Reiss, H.; Heller, A., The absolute potential of the standard hydrogen electrode: a new estimate. *J. Phys. Chem.* **1985,** *89* (20), 4207-4213.
40. Bard, A. J.; Faulkner, L. R., *Electrochemical Methods: Fundamentals and Applications.* John Wiley & Sons: NY, 2000.
41. Robbins, J. L.; Edelstein, N.; Spencer, B.; Smart, J. C., Syntheses and electronic structures of decamethylmetallocenes. *J. Am. Chem. Soc.* **1982,** *104* (7), 1882-1893.
42. Lord, R. L.; Schultz, F. A.; Baik, M.-H., Spin Crossover-Coupled Electron Transfer of $[M(tacn)_2]^{3+/2+}$ Complexes (tacn = 1,4,7-Triazacyclononane; M = Cr, Mn, Fe, Co, Ni). *J. Am. Chem. Soc.* **2009,** *131* (17), 6189-6197.
43. Creaser, I. I.; Harrowfield, J. M.; Herlt, A. J.; Sargeson, A. M.; Springborg, J.; Geue, R. J.; Snow, M. R., Sepulchrate: a macrobicyclic nitrogen cage for metal ions. *J. Am. Chem. Soc.* **1977,** *99* (9), 3181-3182.
44. Endicott, J. F.; Ramasami, T.; Gaswick, D. C.; Tamilarasan, R.; Heeg, M. J.; Brubaker, G. R.; Pyke, S. C., Charge-transfer perturbations of the electronic contributions to bimolecular reactions. Nonadiabatic effects observed in energy-transfer and electron-transfer reactions. *J. Am. Chem. Soc.* **1983,** *105* (16), 5301-5310.
45. Sahami, S.; Weaver, M. J., Entropic and enthalpic contributions to the solvent dependence of the thermodynamics of transition-metal redox couples: Part II. Couples containing ammine and ethylenediamine ligands. *J. Electroanal. Chem. Interfacial Electrochem.* **1981,** *122* (Supplement C), 171-181.
46. Crawford, P. W.; Schultz, F. A., Inner-Shell Effects on Heterogeneous Electron-Transfer Rates of Bis(1,4,7-Triazacyclononane) (tacn) Redox Couples, $M(tacn)_2^{3+/2+}$ (M = Fe, Co, Ni, Ru). *Inorg. Chem.* **1994,** *33* (19), 4344-4350.